

Article

The CYGNO Experiment

Fernando Domingues Amaro¹, Elisabetta Baracchini^{2,3}, Luigi Benussi⁴, Stefano Bianco⁴, Cesidio Capoccia⁴, Michele Caponero^{4,5}, Gianluca Cavoto^{6,7}, André Cortez^{2,3}, Igor Abritta Costa⁸, Emiliano Dané⁴, Giorgio Dho^{2,3}, Emanuele Di Marco⁶, Giulia D’Imperio⁶, Flaminia Di Giambattista^{2,3}, Robert Renz Marcelo Gregorio⁹, Francesco Iacoangeli⁶, Herman Pessoa Lima Júnior¹⁰, Amaro da Silva Lopes Júnior⁸, Giovanni Maccarrone⁴, Rui Daniel Passos Mano¹, Michela Marafini¹¹, Giovanni Mazzitelli⁴, Alasdair McLean⁹, Andrea Messina^{6,7}, Cristina Maria Bernardes Monteiro¹, Rafael Antunes Nobrega⁸, Igor Fonseca Pains⁸, Emiliano Paoletti⁴, Luciano Passamonti⁴, Sandro Pelosi⁶, Fabrizio Petrucci^{12,13}, Stefano Piacentini^{6,7}, Davide Piccolo⁴, Daniele Pierluigi⁴, Davide Pinci^{6*}, Atul Prajapati^{2,3}, Francesco Renga⁶, Rita Joana da Cruz Roque¹, Filippo Rosatelli⁴, Andrea Russo⁴, Joaquim Marques Ferreira dos Santos¹, Giovanna Saviano^{4,14}, Neil Spooner⁹, Roberto Tesauro⁴, Sandro Tomassini⁴ and Samuele Torelli^{2,3}.

¹ LIBPhys, Department of Physics, University of Coimbra, 3004-516 Coimbra, Portugal; famaro@uc.pt (F.D.A.); cristinam@uc.pt (C.M.B.M.); ritaroque@fis.uc.pt (R.J.d.C.R.); RDPMano@uc.pt (R.D.P.M.); jmf@uc.pt (J.M.F.d.S.)

² Gran Sasso Science Institute, 67100, L’Aquila, Italy; andre.f.cortez@gmail.com (A.C.); giorgio.dho@gssi.it (G.D.); flaminia.digiambattista@gssi.it (F.D.G.); atul.prajapati@gssi.it (A.P.); samuele.torelli@gssi.it (S.T.)

³ Istituto Nazionale di Fisica Nucleare, Laboratori Nazionali del Gran Sasso, 67100, Assergi, Italy

⁴ Istituto Nazionale di Fisica Nucleare, Laboratori Nazionali di Frascati, 00044, Frascati, Italy; luigi.benussi@lnf.infn.it (L.B.); stefano.bianco@lnf.infn.it (S.B.); Cesidio.Capoccia@lnf.infn.it (C.C.); caponero@frascati.enea.it (M.C.); Emiliano.Dane@lnf.infn.it (E.D.); giovanni.maccarrone@lnf.infn.it (G.M.); giovanni.mazzitelli@lnf.infn.it (G.M.); Emiliano.Paoletti@lnf.infn.it (E.P.); luciano.passamonti@lnf.infn.it (L.P.); Davide.Piccolo@lnf.infn.it (D.P.); Daniele.Pierluigi@lnf.infn.it (D.P.); filippo.rosatelli@lnf.infn.it (F.R.); arusso@lnf.infn.it (A.R.); giovanna.saviano@cern.ch (G.S.); Roberto.Tesauro@lnf.infn.it (R.T.); sandro.tomassini@lnf.infn.it (S.T.)

⁵ ENEA Centro Ricerche Frascati, 00044, Frascati, Italy

⁶ Istituto Nazionale di Fisica Nucleare, Sezione di Roma, 00185, Rome, Italy; gianluca.cavoto@roma1.infn.it (G.C.); emanuele.dimarco@roma1.infn.it (E.D.M.); giulia.dimperio@roma1.infn.it (G.D.); francesco.iacoangeli@roma1.infn.it (F.I.); andrea.messina@uniroma1.it (A.M.); Alessandro.Pelosi@roma1.infn.it (S.P.); stefano.piacentini@uniroma1.it (S.P.); davide.pinci@roma1.infn.it (D.P.); francesco.renga@roma1.infn.it (F.R.)

⁷ Dipartimento di Fisica, Università La Sapienza di Roma, 00185, Roma, Italy

⁸ Universidade Federal de Juiz de Fora, Faculdade de Engenharia, 36036-900, Juiz de Fora, MG, Brasil; igorabritta@gmail.com (I.A.C.); rafael.nobrega@ufjf.edu.br (R.A.N.);igor.pains@ufjf.edu.br (I.P.); silva.lopes@ufjf.edu.br (A.D.S.L.J.)

⁹ Department of Physics and Astronomy, University of Sheffield, Sheffield, S3 7RH, UK; robert.gregorio@sheffield.ac.uk (R.R.M.G.); ali.mclean@sheffield.ac.uk (A.C.M.L.); n.spooner@sheffield.ac.uk (N.S.)

¹⁰ Brazilian Center for Research in Physics, 22290-180, Rio de Janeiro, RJ, Brazil; herman.lima.jr@gmail.com

¹¹ Museo Storico della Fisica e Centro Studi e Ricerche “Enrico Fermi”, Piazza del Viminale 1, 00184, Roma, Italy; Michela.Marafini@roma1.infn.it

¹² Dipartimento di Matematica e Fisica, Università Roma TRE, 00146, Roma, Italy; fabrizio.petrucci@uniroma3.it

¹³ Istituto Nazionale di Fisica Nucleare, Sezione di Roma TRE, 00146, Roma, Italy

¹⁴ Dipartimento di Ingegneria Chimica, Materiali e Ambiente, Sapienza Università di Roma, 00185, Roma, Italy

* Correspondence: davide.pinci@roma1.infn.it

Citation: Amaro, F.D.; Baracchini, E.; Benussi, L.; Bernardes Monteiro, C.M.; Bianco, S.; Capoccia, C.; Caponero, M.; Cavoto, G.; Cortez, A.; I. A. Costa; et al. The CYGNO Experiment. *Physics* **2021**, *1*, 1–29. <https://doi.org/>

Received:

Accepted:

Published:

Publisher’s Note: MDPI stays neutral with regard to jurisdictional claims in published maps and institutional affiliations.

Copyright: © 2021 by the authors. Submitted to *Physics* for possible open access publication under the terms and conditions of the Creative Commons Attribution (CC BY) license (<https://creativecommons.org/licenses/by/4.0/>).

Abstract: The search for a novel technology able to detect and reconstruct nuclear and electron recoil events with an energy of few keV has become more and more important as long as vast regions of high mass Dark Matter candidate have been excluded. Gaseous Time Projection Chambers (TPC) with optical readout are very promising detector combining the detailed event information

⁵ provided by the TPC technique to the high sensitivity and granularity of last generation scientific light sensors. CYGNO experiment (a CYGNus module with Optical readout) aims at exploiting the Optical Readout approach of multiple-GEM structures in large volume TPC for the study

of rare events as interactions of low mass Dark Matter or solar neutrinos. The combined use of high-granularity sCMOS camera and fast light sensors allows the reconstruction of the 3D direction of the tracks, offering good energy resolution and very high sensitivity in the few keV energy range together with a very good particle identification useful to distinguish nuclear recoils from electronic recoils. This experiment is part of the CYGNUS proto-collaboration which aims at constructing a network of underground observatories for directional Dark Matter search. A 1 cubic meter demonstrator is expected to be built in 2021/22 aiming at a larger scale apparatus (30m³-100 m³), in a later stage.

Keywords: Dark Matter; Time Projection Chamber; Optical Readout

1. Introduction

The presence of in the Universe of large amount of not-luminous matter (usually referred to as *Dark Matter (DM)*) is nowadays an established, yet still mysterious, paradigm [1]. Deciphering its essence is one of the most compelling tasks for fundamental physics today. Electrically neutral and very low interacting particles with a mass in the range between few to thousands of GeV are usually referred to as *Weakly Interacting Massive Particles (WIMPs)*. They represent a well motivated DM candidate, independently predicted by Standard Model extensions and Big Bang cosmology. The measurements of the rotational curve of our Galaxy suggest the presence of a DM halo, through which the ordinary, luminous galactic matter is travelling in its revolution around the Galactic center. This creates a relative motion between an observer on Earth and the particles in the halo, that scientists seek to exploit to detect DM through their elastic scattering with ordinary matter. In particular, nuclear recoils are expected to be the clearest evidence of WIMP interactions.

Given their rarity, the main experimental challenge of direct DM searches in the GeV mass region is to discriminate the very low energy nuclear recoils (1-100 keV) from interactions induced by other particles, which have largely higher rates. The apparent WIMP wind would create two peculiar effects for an observer on the Earth, that can be exploited for a positive identification of a DM signal. Since in its rotation around the Sun the Earth orbital velocity is anti-parallel to the DM wind in summer and parallel in winter, the observed DM rates inside the detector are expected to display a seasonal modulation of few percent. A much more robust signature is provided by the diurnal directional modulation of the DM signal. The peak flux, in fact, comes from the direction of solar motion around the center of our Galaxy, which happens to point towards Cygnus constellation. Due to the Earth rotation around its axis (oriented at 48° with respect to the direction of the DM apparent wind), an observer on Earth would see the average DM incoming direction changing of ~ 96° every 12 sidereal hours. The amplitude of the modulation depends on the relative angle between the laboratory frame and the Earth axis, with the maximum at 45° inclination and no modulation along directions parallel to the axis.

The determination of the incoming direction of the WIMP can therefore provide a correlation with an astrophysical source [2] that no background can mimic. Directional measurement can furthermore discriminate between various DM halo models and provide constraints on WIMP properties, like no other non-directional detector[2].

While the last few decades have seen enormous advances in direct DM search, leading to many orders of magnitude improvement for masses larger than 10 GeV, the O(GeV) mass range still remains theoretically well motivated and largely unexplored to these days [3]. Given the kinematic of the elastic process, a direct DM detection experiment achieves its best sensitivity for WIMP masses equal to the target mass nuclei. The maximum fraction ϵ of the energy that can be transferred to a target of mass m_T by a WIMP of mass m_χ is in fact given by:

$$\epsilon = \frac{4\rho}{(\rho + 1)^2} \quad (1)$$

with $\rho = \frac{m_T}{m_\chi}$. Therefore, low mass target nuclei, such as Hydrogen and Helium, are the best choices to maximise the sensitivity to O(GeV) WIMP masses.

The CYGNO experiment hence proposes an innovative approach to the direct DM search challenge. A high resolution 3D gaseous Time Projection Chamber (TPC) operated at atmospheric pressure is employed with light target nuclei such as Helium and Fluorine, to boost the sensitivity to O(GeV) WIMP masses for both Spin Independent (SI) and Spin Dependent (SD) coupling. It is also important to notice that light target nuclei will result in longer track lengths, easing the determination of their direction providing direction sensitivity. Studies to add a hydrogen-based gases to provide even lighter targets are ongoing. The topological signature of the recoil event improves also particle identification and hence rejection of annoying backgrounds down to low energy thresholds. The possibility of operation at atmospheric pressure guarantees a reasonable volume to target mass ratio, while at the same time allowing to reduce the requirements on the vessel (hence internal backgrounds). The possibility of a high resolution 3D TPC, such as the one foreseen by this project, will allow CYGNO to explore new physics cases that possess such signature. This include, among the others, the elastic scattering of sub-GeV DM [4] and of solar neutrinos [5,6].

The results obtained with current prototypes (Sec. 3) are the basis for the designs of a 1 m³ demonstrator (CYGNO PHASE_1), that is the subject of this paper. According to the performance of this, the collaboration will propose a larger detector for a competitive experiment (CYGNO PHASE_2). With this program, CYGNO fits in the context of the wider international CYGNUS effort, to establish a Galactic Directional Recoil Observatory that can test the DM hypothesis beyond the Neutrino Floor and measure the coherent scattering of neutrinos from the Sun and Supernovae[7].

2. CYGNO Experimental Approach

The CYGNO experiment goal is to deploy at Laboratori Nazionali del Gran Sasso a high resolution TPC with optical 3D readout based on Gas Electron Multipliers (GEMs) working with a Helium/Fluorine gas mixture at atmospheric pressure for the study of rare events with energy releases in the range 1-100 keV.

Although challenging, gaseous TPCs constitute a promising approach to directional DM searches providing a set of crucial observables:

- TPC are usually made by a sensitive volume, filled with gas or liquid, enclosed between an anode and a cathode generating a suitable electric field in it [8–10]. The passage of a ionising particle, produces free electrons and ions that start to drift toward the above mentioned electrodes. These are usually segmented and properly readout to provide a granular information about the charge collection point on the plane. The third coordinate can be evaluated from the drift time measurement. Therefore, TPC are inherently 3D detector capable to acquire large sensitive volumes, with a lower amount of readout channels with respect to other high precision 3D tracking systems.
- Gaseous detectors can feature very low energy detection thresholds. In gas, a single electron cluster can be produced with energy releases of the order of few tens of eV and this has a very good chance of reaching the multiplication region and to produce a detectable signal.
- A measurement of the total ionisation indicates the energy released by the recoil and (depending on the readout plane granularity) the profile of the energy deposit along the track can be measured with high precision, providing excellent background discrimination.

- The track itself indicates the axis of the recoil and the charge profile along it encodes the track orientation (*head-tail*), providing an additional powerful observable for DM searches.
- Large choice of gases can be employed in a TPC, from light to heavy nuclei, with both odd and even spins, therefore sensitive to both SI and SD interactions also in the low O(GeV) mass region.
- A room-temperature and atmospheric-pressure detector results in operational and economical advantages, with no need for cooling or vacuum sealing. These choices allow for a much more compact experiment realization and straightforward scaling when compared to cryogenic solutions currently dominating the DM direct search scene.
- TPCs up to 100 m³ of active volume have already been successfully operated [11,12] and up nearly 20000 m³ approved for construction in the neutrino field [13], showing the feasibility of very large detectors with large active masses.

120 2.1. CYGNO Optical Readout

Gas luminescence is a well studied and established mechanism: charged particles traveling in the gas can ionize atoms and molecules but can also excite them. During the de-excitation processes, photons are emitted. Amount and spectrum of light produced strongly depends on the gas, on its density and the possible presence and strength of an electric fields [14–16].

The idea of detecting the light produced during the multiplication processes, proposed many years ago [17], has received in recent years a renewed attention. The optical readout approach, in fact, offers several advantages:

- highly performing optical sensors are being developed for commercial applications and can be easily procured;
- light sensors can be installed outside the sensitive volume reducing the interference with high voltage operation and the gas contamination;
- the use of suitable lenses allows to image large O(1) m² areas with a single sensor while maintaining O(100) μm effective pixels transverse size.

In recent years, an increasing number of tracking detectors have started employing Micro-Pattern Gaseous Detectors (MPGDs). Their major advantages are the very high achievable granularity and rate capability, together with mechanical robustness. The production technology for MPDG guarantees nowadays very high quality devices, providing stable and uniform operation. In particular Gas Electron Multipliers (GEMs) [18] have already been used to equip very large areas with high space and time resolution [11], and have more recently been employed coupled to pixelised light sensors showing very good performances [14,19–21] (see also Sec.3).

Charge Coupled Devices (CCD) have been widely used in the past as high granularity light sensors for optical TPC approaches [21–23]. CCDs main limitation for the study of rare events in the 1-100 keV energy range is represented by the high level of readout noise, up to 5 to 10 electrons rms per pixel. More recently, cameras based on CMOS technology have been developed, that can reach tens of millions of pixels, with very low readout noise (less than 1 electron rms per pixel), sub-electron readout noise and single photon sensitivity.

The CYGNO collaboration proposed the introduction of CMOS based optical devices for GEM detector optical readout in 2015 [24]. The high sensitivity of this technique resulted in a very good performance in the particle detection not only at the energies of interest for DM searches (as is illustrated in Sec.3), but also for minimum ionising particle, from both cosmic rays and high energy electrons [20,25–28].

Because the current frame rate available for CCDs or CMOS is still low compared to the temporal extent of typical TPC signals, such devices can provide only 2D projection of the recoil track. In order to achieve 3D track reconstruction, the CYGNO experiment aims at complementing the CMOS image information with the signal of a fast light

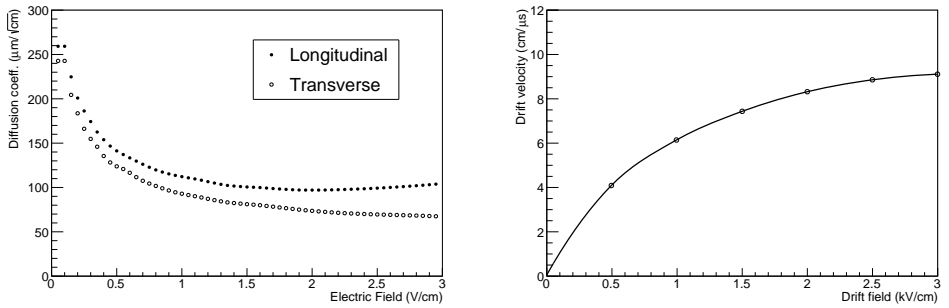


Figure 1. Transverse and longitudinal diffusion coefficients for He/CF₄ 60/40 (left) and electron drift velocity (right) as a function of the drift field.

sensors (PMT or SiPM), that can provide the track profile along the drift direction (see Sec.3).

2.2. CYGNO Gas Mixture

The relative photon yield, defined as the ratio between the number of produced photons and the total number of secondary electrons produced in the avalanche process, and in general the overall detector performances, are significantly dependent on the gas characteristics: ionization statistics, transport properties (drift velocity and diffusion), electron multiplication and light production. In the context of optical TPCs for DM searches, CF₄ is a particularly interesting gas because of its well known properties as efficient scintillator, and the large fluorine content that provides sensitivity to spin-dependent WIMP-proton interactions. It was demonstrated by previous studies [14] that CF₄-based mixtures have electro-luminescence emission spectra with a large peak around 600 nm, where Si-based sensors (CCD or CMOS) offer their highest quantum efficiency.

For these reasons, He/CF₄ mixtures in different proportions were extensively studied within the CYGNO project. The best performance were found for a mixture with 60% Helium and 40% CF₄ [29,30]. The behaviors of the diffusion coefficients and drift velocity for different electric fields were calculated with Garfield [31,32] and are shown in Fig. 1.

An estimate for the average energy loss per single ionization of 42 eV was also evaluated. As it can be seen from Fig. 1, a remarkable additional advantages of the use of CF₄ is the small electron diffusion, that can provide a reduced deterioration of the track original shape.

The effective ranges of electron and He-nuclei recoils were simulated respectively with GEANT4 [33] and SRIM software¹. The 2D projected ranges on the readout plane (i.e. the CMOS camera image) as a function of particle kinetic energy are shown in Fig. 2:

- He-nuclei recoils have a sub-millimetre range up to energies of 100 keV and are thus expected to produce bright spots with sizes mainly dominated by diffusion effects;
- low energy (less than 10 keV) electron recoils are in general larger than He-nuclei recoils with same energy and are expected to produce less intense spot-like signals. For a kinetic energy of 10 keV, the electron range becomes longer than 1 mm and for few tens of keV, tracks of few centimetres are expected.

3. Experimental Results with CYGNO Experiment Prototype

The experimental results obtained with the prototype named Long Elliptical MOdule: LEMON represents the most comprehensive example currently available of the

¹ Visit the <http://www.srim.org/> site for more information

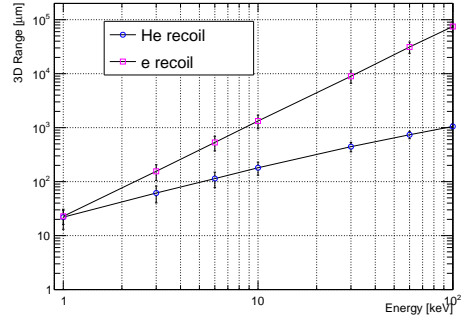


Figure 2. Average 2D projected ranges on the readout plane for electron and He-nuclei recoils as a function of their kinetic energy.

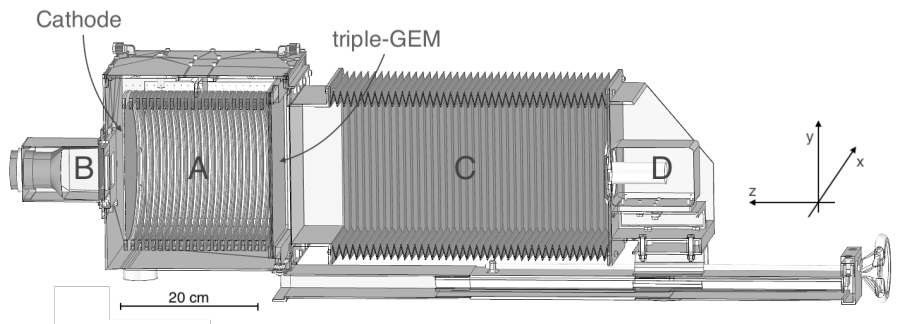


Figure 3. The LEMON prototype [35]. The elliptical sensitive volume (A), the fast photo-multiplier (B), the optical bellow (C) and the sCMOS-based camera (D) are indicated.

performance achievable with the CYGNO approach. The LEMON detector, shown in Fig. 3, is schematically composed by:

- a gas sensitive volume of 7 litres contained in a 20 cm long cylindrical field cage (FC) with an elliptical base with 24 cm and 20 cm axes;
- a $24 \times 20 \text{ cm}^2$ stack of three GEM as the amplification stage facing the CMOS camera;
- a mesh-based semitransparent cathode closing the volume on the opposite side, behind which a PMT is placed;

A more detailed description of this prototype can be found in Ref.[34] and [28].

LEMON standard operating conditions were based on following sets:

- an He/CF₄ (60/40) gas mixture flux of 200 cc/min;
- an electric drift field within the sensitive volume $E_D = 0.5 \text{ kV/cm}$;
- an electric transfer field in the 2 mm gaps between the GEMs $E_{\text{Transf}} = 2.5 \text{ kV/cm}$;
- a voltage difference across the two sides of each GEM $V_{\text{GEM}} = 460 \text{ V}$;

According to results presented in [30], in this configuration an electron multiplication of about 1.5×10^6 is expected.

- As anticipated in Sect. 2.1, high quality cameras are a crucial ingredient for the experiment results An ORCA Flash 4.0 camera² was selected to equip LEMON. This device is based on a $1.33 \times 1.33 \text{ cm}^2$ scientific CMOS sensor, subdivided in 2048×2048 pixels with an active area of $6.5 \times 6.5 \mu\text{m}^2$ each, with a quantum efficiency of 70% at 600 nm and a readout noise of 1.4 electrons rms. The response and noise level of this sensor were tested with a calibrated light source [20]. A response of 0.9 counts/photon was measured together with a rms fluctuation of 1.3 photons/pixel.

² For more details visit www.hamamatsu.com

In order to image the large GEMs surface, the camera is equipped with a Schneider lens with 25.6 mm focal length f and 0.95 aperture a . Since at a distance d the lens provides a de-magnification of:

$$\delta = \frac{f}{d-f} \quad (2)$$

the camera optical system is placed at $d=52.6$ cm distance from the GEMs, in order to image a 26×26 cm² area. The solid angle covered by the sensor, which in turn determine the geometrical acceptance of photons is given by

$$\Omega = \frac{1}{(4(1/\delta + 1) \times f)^2}$$

resulting in 1.57×10^{-4} for the LEMON layout. This is the price the optical readout approach needs to pay in order to image large areas, and that clarifies why high electron gain gas mixtures are needed to reach low energy detection thresholds.

In order to complement the 2D track projection recorded by the CMOS with the track trajectory along the drift direction, the arrival time profile of the primary electrons could be extracted from the signal induced on the third GEM bottom electrode. Nonetheless, this is expected (and explicitly shown in [25]) to suffer from a considerably large noise (typically due to jitter on the high voltage supply line), that could prevent signal detection at the low energies at play.

To overcome this limitation, light track time profile was concurrently readout by a Photonics XP3392 Photo Multiplier Tube (PMT) with a 5 ns rise-time, a maximum QE for 420 nm and a 76 mm square-window, providing sensitivity to single photon and significant reduced noise with respect to the GEM electric signal.

Performance of LEMON were tested in recent years at Laboratori Nazionali di Frascati of INFN (LNF) overground laboratory by means of radioactive sources (⁵⁵Fe, AmBe), high energy (400 MeV) electrons from a beam at the BTF facility [36,37] and cosmic rays, and are summarised in the following.

3.1. Operation Stability

The performance and long term stability of LEMON was tested for a month long run, during which the detector was exposed to environmental radioactivity, cosmic rays and a ⁵⁵Fe source [29]. During the whole period, all currents drawn by the high voltage channels supplying the electrodes of the GEM stack were monitored and recorded to identify sudden and large increases that could indicate discharges or other electrostatic issues.

During the test, two different kinds of electrostatic instabilities were observed:

- hot-spots appearing on the GEM surface. While in some cases these would fades out with time, sometimes they started to slowly grow up to tens of nA (on a time scale of minutes). These are very likely due to self-sustaining micro-discharges happening in one or few GEM channels.
- high charge density due to very high ionizing particles or charge accumulation on electrode imperfections can suddenly discharge across GEM channels. In these events, a sudden increase in the drawn current is recorded with a voltage restoring on the electrodes through protection resistors on a few seconds time basis. Even if these events are less frequent than hot spots, they can be dangerous for the GEM structure and the energy released in the discharge can, in principle, damage it.

An automatic recovery procedure was implemented, triggered by the raising of the GEM currents, able to recover both hot-spots and discharges by lowering and gradually restoring the GEM voltages operating conditions in few minutes.

An average of 16 of such instabilities were observed per day and the total dead time introduced by the recovering procedures was less than 4%. A detailed analysis of the time distance between two consecutive phenomena did not show any correlation

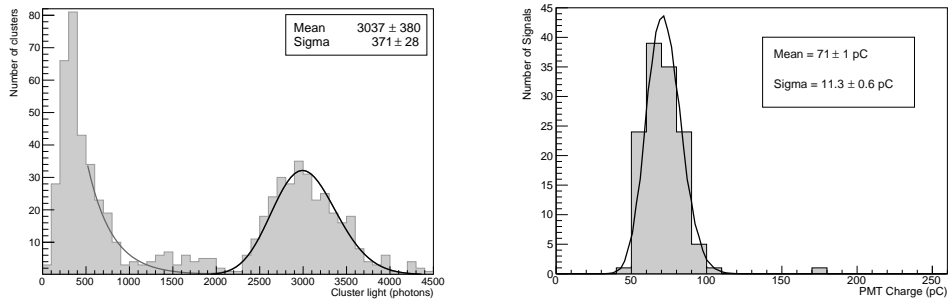


Figure 4. Distribution of the light content of the ^{55}Fe events reconstructed from the sCMOS images (left) and distribution of the charge measured by the PMT signals (right).

260 between two subsequent events, nor any increase of their rates. This allowed to conclude that detector operation looked very safe and stable and the obtained performance was completely satisfactory. Different gas proportion were tested and a lower amount of CF_4 resulted in a less stable electrostatic configuration.

3.2. Light Yield and Energy Resolution

265 The light production was evaluated by analysing CMOS and PMT response to interactions in gas of 5.9 keV X-rays produced by a ^{55}Fe source. The CMOS images were acquired in free running mode (i.e. without using any trigger signal) with an exposure of 100 ms. The CMOS pixels pedestal noise was extracted from the average of 100 images acquired in absence of any light signal and subtracted to each image before the analysis.
270 An elementary clustering algorithm based on nearest neighbor-cluster (NNC) is applied to 4×4 rebinned images to select ^{55}Fe like events.

Figure 4 shows on the left the light spectrum of the ^{55}Fe events reconstructed from the sCMOS images and on the right the integral of the charge signal measured by the PMT.

275 The average light yields were evaluated from a Polya fit [38] to the two distributions, resulting in:

- an average of 514 ± 63 detected photons per keV released in the gas by the sCSMOS camera (in agreement with results obtained with lower V_{GEM} and E_{Transf} [34]), with an energy resolution of 12%;
- 280 • an average of (12.0 ± 0.2) pC per keV released in the gas with an energy resolution of 16% from the PMT charge signal;

3.3. Detection Efficiency

285 The detection efficiency along the whole 7 litres sensitive volume was studied acquiring CMOS images varying a collimated ^{55}Fe source distance from the amplification plane and the electric drift field strength within the field cage Figure 5 shows on the left the number of reconstructed ^{55}Fe spots in the CMOS images with the algorithm illustrated in Sec.3.2 as a function of drift field E_D , normalized to the value obtained for $E_D = 600$ V/cm. For E_D larger than 300 V/cm a plateau is found, indicating a full detection efficiency for larger field values. Right panel of Fig. 5 shows the dependence 290 of n on the source distance from the GEM amplification plane, normalised to its average value \bar{n} . A constant behavior is found in all tested positions, allowing to conclude that detection inefficiency is negligible down to 6 keV energy deposit.

3.4. Track absolute distance along the drift direction

295 The possibility to determine the absolute z position of the event in electron drift was studied with 450 MeV electrons from the LNF-BTF facility [28]. The transverse diffusion in the drift gap can in fact be exploited to extract the drift length and thus infer the absolute z distance at which the track occurred.

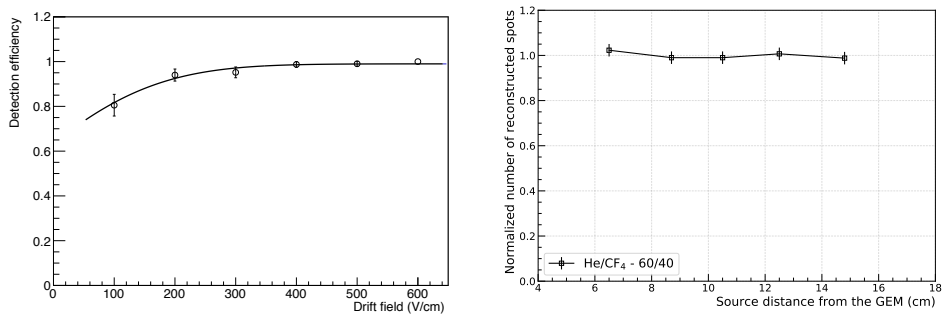


Figure 5. Behavior of the normalized number of ^{55}Fe spots as a function of drift electric field (left) and event depth in sensitive volume (right).

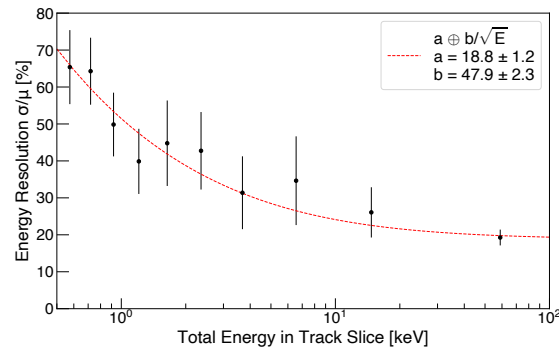


Figure 6. Behavior of the relative fluctuation of the energy measured in track segments of different length.

Short 7 mm long track segments (having an average energy deposit of 1.5 keV given the energy loss expected for 450 MeV electrons) were used to evaluate the detector performance for small energy releases. Figure 6 shows that a 40%-50% energy resolution is achievable for such short segment (i.e. of the order of 1 keV), with a position resolution between 100 μm (near the GEM plane) and 300 μm (20 cm far from GEM plane).

As described in [35], the light profile transverse to the track direction possesses a Gaussian shape with the total light being proportional to $\sigma_{light} \times A_{light}$ (where σ_{light} is the sigma and A_{light} the amplitude of the Gaussian). In the assumption of an electron absorption length λ in the drift path and since diffusion increases as \sqrt{z} , the ratio $\eta_{light} = \sigma_{light} / A_{light}$ is expected to grow quadratically with the drift distance [28].

Similarly, longitudinal electron diffusion modifies the electron time of arrival on the GEM and thus the time structure of the signal recorded by the PMT. Also in this case, the ratio $\eta_{time} = \sigma_{time} / A_{time}$ between the amplitude and the width of the time waveform is expected to increase with z .

Figure 7 shows the dependence of η_{light} and η_{time} as a function of z with a superimposed linear fit.

These observables can be therefore used to evaluate the absolute z with about 15% uncertainty over 20 cm length [28].

These features result crucial in selecting the fiducial signal volume and therefore rejecting annoying backgrounds coming from radioactivity of TPC materials, like cathode or GEMs.

3.5. Detection and Identification of Nuclear and Electron Recoils

Thanks to the detailed information provided by the high granularity optical sensors, track properties like shape, size, light density and so on can efficiently be exploited to identify and separate Nuclear Recoils (NR) expected from a DM signal from Electron Recoils (ER) coming from background sources.

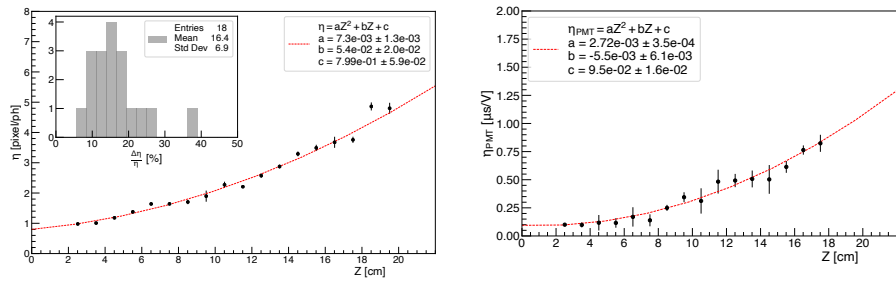


Figure 7. Dependence of η_{light} on left and η_{time} on the right as a function of the track distance from the GEM (see text for details).

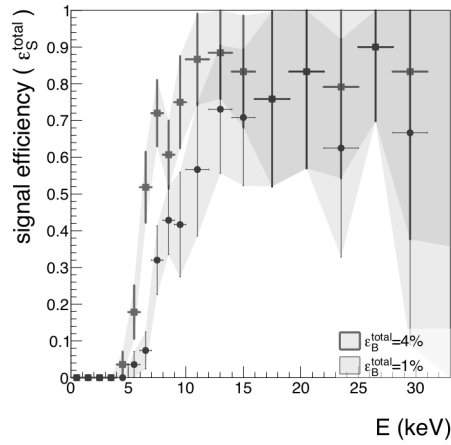


Figure 8. Detection efficiency for nuclear recoils as a function of their detected energy for electron recoils rejection of 96% (squares) and 99% (circles).

To quantify these features within CYGNO experimental approach, a track reconstruction and identification algorithm was developed for the analysis of the sCMOS images, called iDBSCAN [39] and based on an adapted version of the well-known Density-Based Spatial Clustering of Applications with Noise (DBSCAN) [40]. The iDBSCAN, exploiting the number of photons in each pixel as a third dimension to the phase space of the points considered, separately identifies clusters displaying different intensity (i.e. energy deposition patterns), and therefore likely belonging to different classes of particles interactions.

The performance of the algorithm were studied on 5.9 keV energy deposit from ^{55}Fe and NR produced by an AmBe source [41]. The 59 keV $_{ee}$ photons produced by AmBe were nearly completely shielded by a lead shield built around the detector. Data were taken overground at LNF and were therefore highly contaminated by cosmic ray particle interactions.

In order to select a pure sample of nuclear recoil candidates produced by the interaction of the neutrons originating from the source and to identify various sources of backgrounds, several cluster shapes observables were exploited. Among these, the *slimness* (ζ) was used to mainly distinguish cosmic rays and the light *density* (δ) to discriminate electron from nuclear recoils. The slimness is the ratio of the Gaussian width of the track in the transverse direction over the projected path length. The density is the ratio of the total number of photons detected by all the pixels gathered in the cluster over the total number of pixels.

Exploiting a simple selection on δ , an ER background rejection in the energy region around 5.9 keV $_{ee}$ of 96.5% (99.2%) was found together with 50% (40%) NR efficiency [41].

While this cut-based approach is minimalist, and could be improved by more sophisticated analyses combining several topological variables and also the information from PMT waveforms, it shows that a rejection factor larger than 10^2 for electron recoils at $E = 5.9$ keV can be obtained with a gas detector at atmospheric pressure, while retaining a high fraction of NR event signals.

4. The CYGNO experiment roadmap and synergies

The CYGNO project will be developed through a staged approach, to optimise the apparatus and improve its performance while better mitigating any unexpected contingency.

This roadmap, will comprise of:

- PHASE_0: measuring the performances of a 50 litres prototype, while at the same time testing materials, construction techniques and auxiliary systems;
- PHASE_1: proving the potentialities and the scalability of the experimental approach on a $O(1)$ m³ detector;
- PHASE_2: exploring the 1-10 GeV WIMP mass region *with directionality capabilities* and high sensitivity for both SI and SD couplings and the possibility of performing the first measurement of low energy solar neutrinos with directional information.

The roadmap details and synergies with other projects will be illustrated in the following.

4.1. CYGNO PHASE_0: the LIME prototype

The Long Imaging ModulE (LIME, in Fig. 9) is equipped with triple 33×33 cm² thin GEMs (stretched on plexiglass frame to reduce radioactivity), amplifying a 50 cm drift length, for a total active volume of about 55 litres imaged by 4 small PMT and a single sCMOS. The new Hamamatsu ORCA-Fusion Camera was employed³ with improved performance with respect to the Orca Flash (see Sec.3) in terms of reduced noise (0.7 versus 1.4 electrons), larger number of pixels (2304×2304 versus 2048×2048) and larger quantum efficiency (80% versus 70% at 600 nm). The choice of 4 PMT resides in the possibility of better reconstructing track position and inclination through center of gravity of the light signal from the 4 sides, strongly mitigating any possible pile up effect.

The gas volume is enclosed in a 10 mm thick plexiglass box, that provides gas tightness. The field cage is composed by copper rings, conveniently roundly shaped to avoid discharges, at a 1 cm pitch (see Sec.4.2).

In its underground installation LIME will be equipped with the same DAQ system and gas system envisaged to be employed for the realisation of PHASE_1, currently under test.

A response of 1180 ph/eV (to be compared with 514 ph/eV obtained with LEMON, see Sec.3.2) was measured effectively lowering our energy threshold of a factor 2. The energy resolution on the ^{55}Fe peak is measured to be 14% across the whole 50 cm drift length, with full efficiency in the full 50 litres volume. LIME has been furthermore already operated for one entire month in He/CF₄ 60/40 at 1 atm, with its currents continuously monitored and logged, showing comparable stability to LEMON (see Sec. 3.1).

The PHASE_1 demonstrator will be based on readout modules having the LIME dimensions and layout (see Sec.4.2). For this reason, its successful assembly and operation will be paramount to substantiate the efforts and confirm the scientific and technological choices towards the 1 m³ detector.

³ <https://www.hamamatsu.com/eu/en/product/type/C14440-20UP/index.html>

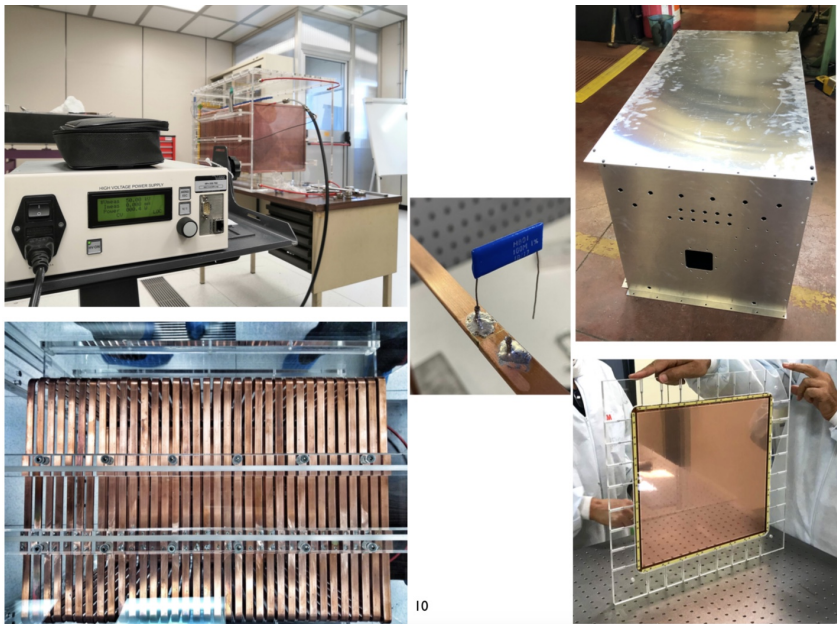


Figure 9. Picture of the LIME detector assembly at Laboratori Nazionali di Frascati: top left with drift field and GEM operating at nominal voltages, bottom left detail of the field cage copper rings, center detail of the resistor soldered to the field cage ring, top right LIME inside the Faraday cage, bottom right detail of the triple GEM stretched with pullouts on a plexiglass frame.

The installation at LNGS, completed with the PHASE_1 auxiliary systems, will allow to test on realistic dimensions and operating conditions the construction and material options, and detector long term activity in the underground environment.

In addition, two modes of operation are foreseen at LNGS, each with its own specific scientific goal:

- **Environmental neutron flux measurement operation.** LIME will be equipped with an electromagnetic background shielding of about 10 cm of Copper, to reduce external gamma backgrounds. The goal of this first stage is to demonstrate the capability to precisely track low energy nuclear recoils in an underground setup by measuring the environmental underground neutron flux with directionality. While already fundamental for the successive PHASE₁ development, this measurement will provide a crucial input for any present and future rare events search experiment at LNGS.
- **Internal electromagnetic background measurement operation.** An additional Water shielding of about 50 cm will be added to the Copper shielding, in order to avoid external neutrons interacting in the detector active volume. The combination of Water/Copper/Lead shielding must ensure a level of background contamination inside the detector smaller than the one expected from its internal components, that from current estimations are expected to be about $0.5 - 1 \times 10^5$ per year in [1,20] keV_{ee} range (see Sec.4.2). With this configuration, it will be therefore possible to precisely assess the background assay to further minimise it through material and shielding choices for PHASE_1.

4.2. CYGNO PHASE_1: the O(1) m³ demonstrator

The PHASE_1 detector will comprise of O(1) m³ active gas volume, with two back-to-back TPCs separated by a central aluminised mylar cathode following the DRIFT example [42], able to minimise backgrounds induced from Radon Progeny recoils. The exact PHASE_1 detector sizes is still under discussion, anyway a 1 m³ active volume will be discussed in this paper, schematically shown in Fig. 10, with the consideration

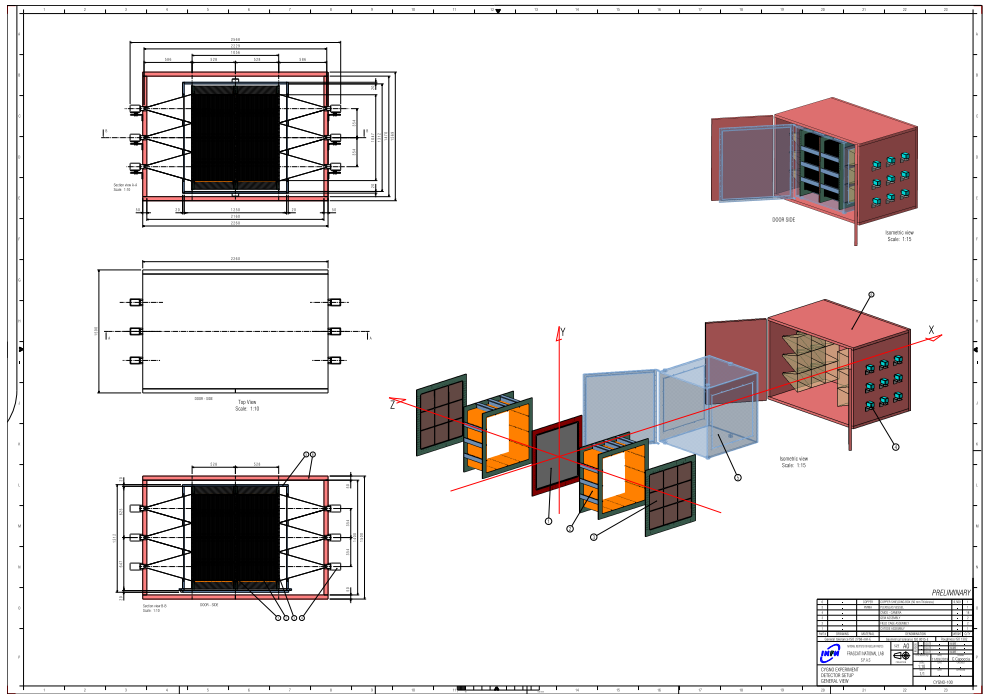


Figure 10. CYGNO PHASE_1 Sensitive Detector Layout

that the foreseen layout and auxiliary system can be directly and easily adapted to the definitive detector dimensions.

The active volume of the detector will be contained in a gas volume vessel (GVES), realized with PMMA to lower the material intrinsic radioactivity, gas contamination and ensure the electrical isolation from cathode and field cage. The box will contain two field cages 500 mm long, separated by a central cathode. On the two endcaps, two arrays of triple GEM will be located, to amplify the signal generated in the gas. Each endcap will be readout by N modules of $33 \times 33 \text{ cm}^2$ area, each one equipped with a sCMOS and 4 PMT, identical to the LIME prototype of PHASE_0, where N depends on the final detector dimension. For a 1 m^3 , 9 LIME-like modules are foreseen for each end cap, for a total of 18.

The GEMs will be assembled adapting the technique discussed in [43]. The mechanical rigidity will be provided by the outer frame that will be anchored to the GVES. The outer frame will support the stretching screws pulling the GEMs to produce the necessary mechanical tension (0.1 N/m applied by mean of dynamo-metric screwdriver) to ensure flatness and homogeneous electric field between the foils [44]. The assembled GEM stack will be inserted into the GVES through vertical slits, which will allow and easy substitution of a single GEM foil in case of damage.

The high voltage system has been conceived with the assumption of independent lines for each electrodes of the GEM foils, in order to ensure safe and reliable operation of the detectors. Since for a 1 m^3 18 \times 3 GEMs are foreseen, a total number of 108 independent high voltage channels has been considered for PHASE_1. The baseline adopted solutions is based on boards equipped with 14 Floating Channels.

The DAQ system needs to be able to collect synchronized data from cameras and photodetectors and to handle the following specifications:

- camera exposure from 0.2 to 1 second (1 to 5 Hz frame rate);
- 10 MB of data per picture (5 MP, 16 bit per pixel);
- 450 12-bit digitization of photodetector waveforms at $\sim 250 \text{ MS/s}$ in $\lesssim 1 \mu\text{s}$ windows.

Since sCMOS cameras data can not be used to develop a trigger, the only possible sources of signals to start data acquisition are from the photodetectors. The possibility of running either in trigger or trigger-less mode was also evaluated.

Component	^{238}U (^{234m}Pa)	^{238}U (^{226}Ra)	^{235}U	^{232}Th (^{228}Ra)	^{232}Th (^{228}Th)	^{40}K
Camera body [Bq/pc]	7	1.8	0.4	2.1	2.1	1.9
Camera lens [Bq/pc]	0.9	0.41	0.031	0.08	0.08	11
GEM foil [Bq/m^2]	< 0.104	0.004	< 0.002	< 0.004	< 0.002	< 0.045
Acrylic [Bq/kg]		0.003		0.005	0.004	0.035

Table 1: Measured activity of the internal detector components expected to produce the largest backgrounds in the active volume. The isotopes in parentheses indicate the activity from that particular part of the decay chain. Upper limits are given at 90% confidence level.

The acquisition will be distributed through a few machines to ensure stability
 455 of the system. To acquire fast photodetectors, digitization boards are considered. In this scenario, the bottle-neck for the acquisition would be the throughput to the disk, typically limited to $O(200 \text{ MB/s})$, and some pre-selection of the images by a farm of CPUs would be needed.

4.2.1. PHASE_1 Shielding Scheme and Material Budget

460 A GEANT4 based Montecarlo simulation reproducing a 1 m^3 detector as from the engineering design of Fig. 10 has been developed to study external and internal background and to optimise the choice of shielding and materials.

465 The effect of the diffused external environmental γ and neutron flux using as a reference the spectra measured at LNGS was studied. Different configurations of external passive shielding with layers of Copper, Lead and Water were studied with the goal of less than 10^4 gamma/year interacting in the target gas between 1 keV and 20 keV. The choice of this benchmark is backed up by indication from measurements[45,46] and simulation within the CYGNUS collaboration[7] that a TPC with 3D readout can reach a 10^5 gamma/year rejection factor at $O(\text{keV})$.

470 While the use of Pb can significantly reduce the overall setup dimensions, the simulation showed that this configuration would require archaeological Lead in order not to induce additional background from the shielding, therefore largely raising the cost of this layer. A cost-benefit optimisation of the shielding layer materials and thicknesses was hence developed, identifying 2 m of Water + 5 cm of Copper as the optimal configuration. This shielding provides an attenuation of about 10^{-7} for external gammas and 5×10^{-5} for external neutrons, reducing the number of expected electron recoils in the active volume below 10^3 cpy (with $O(1)$ cpy nuclear recoils) in the range 1-20 keV.

480 For the evaluation of the internal backgrounds generated by detector materials, the natural gamma radioactivity of the components expected to give the largest contributions was experimentally measured with high purity Germanium detectors thanks to the support of LNGS Special Techniques Service and are reported in Table 1.

485 Regarding the GEMs, the major source of background is found to come from the frames rather than the foils themselves. For this reason, in the LIME prototype of PHASE_0 the triple $33 \times 33 \text{ cm}^2$ GEMs were mounted and stretched on low radioactivity acrylic frames, with same technique foreseen to be applied to the PHASE_1 detector.

490 For what concerns the sCMOS optical system, a large ^{40}K contamination was observed in the objective glass. Suprasil was selected as an alternative material for the fabrication of the lens, for an expected $\sim 10^4$ reduction of the contribution from this item. An overall activity of less than 50 mBq/kg was found in recent measurements performed on a sample at LNGS, confirming the very good properties of this material.

495 sCMOS cameras have never been employed yet in DM searches, and therefore their intrinsic radioactivity has never been studied or optimised in this context. For this reason, an extensive program working in close contact with sCMOS camera producer companies and with LNGS Services to assess this aspect within our experimental approach has started. Gamma spectroscopy of several sCMOS cameras as a whole was

performed, including models from companies different from Hamamatsu, and verified that all displays similar activities in the $O(10)$ Bq/piece. The measured activities of the Hamamatsu Orca Fusion are shown in Table 1. A camera was disassembled in
 500 20 different pieces, which are currently under measurement in order to pin point the components introducing the larger radioactivity contamination and possibly substitute them with cleaner options. Given the very large sCMOS activity, in the PHASE-1 design they are foreseen to be shielded by the 5 cm Copper layer on all sides, except for the one facing the GEM.

505 Starting from these considerations, a background evaluation for a 1 m^3 PHASE-1 detector was developed, that includes the external gamma and neutron flux contribution with the Copper + Water shielding discussed above, and the radioactivity contribution of the main internal components. For this last, the values measured at LNGS for GEMs, camera objective, camera body and acrylic for the gas vessel, and data from literature
 510 for the Cu of the cathode and the field cage rings [CIT] were employed. This study showed that $O(10^3)$ nuclear recoils and $O(10^6)$ electron recoils per year are expected in the sensitive volume, with energy in the 0-20 keV range. It must be noted that all the nuclear recoils are produced by the GEMs and are absorbed in the gas within 5 cm from them. As it is described in Sect. 3.4, by exploiting the effect of diffusion in gas, the track
 515 absolute distance from the GEM can be evaluated with a resolution better than 20%. Therefore, this NR background is expected to be reduced to zero with a suitable selection on the drift distance, without a significant reduction of the detector fiducial volume. The largest amount of electron recoils is produced by the sCMOS cameras, if the camera objective can me made of a clean material, and at a second order by the GEMs.

520 This study represents the current evaluation of the expected backgrounds for a 1 m^3 detector, which can be further minimised by the material screening and the study of the sCMOS intrinsic radioactivity ongoing, and do not therefore need to be considered the ultimate achievable performances.

525 4.3. CYGNO PHASE_2

The experimental results and sensitivities measured on the 1 m^3 demonstrator, will provide crucial information about the possibility of proposing a larger experiment.

A development of such a detector in terms of intrinsic background minimisation and tracking performance, would of course require an improved scalable design in terms
 530 of active volume versus readout area and costs. The possible improvements include, but are not limited to, the following:

- development of custom sCMOS sensors, with faster frame rate, lower noise, improved granularity, improved QE over a wider wavelength spectrum and reduced intrinsic radioactivity.
- enhancement of the light yield through optimised amplification stage with reduced intrinsic radioactivity, possibly including the exploitation of the electroluminescence recently demonstrated by the CYGNO collaboration in He/CF₄ [47];
- optimisation of the optical configuration, to possibly strongly reduce the costs. Due to the very low rate the probability to have multiple events in different area of the
 540 detector is very low. This implies that many areas of the GEMs active surface can be observed simultaneously by the same sensor by multiplexing the image with mirrors or collecting different area in on the same focus point with collimators. Studies of this concept are ongoing;
- reduction the intrinsic detector material radioactivity, with the lesson learned after the results obtained with PHASE-1.
- boost of tracking performances through the development of innovative gas mixtures for optical readouts that will be illustrated in the following sub-section.

4.4. INITIUM: an Innovative Negative Ion Time projection chamber for Underground dark Matter searches

550 The challenging goal of INITIUM is to develop Negative Ion Drift (NID) operation within the CYGNO optical approach.

555 Negative Ion Drift is a peculiar modification of conventional TPCs (NITPC) that involves the addition to the gas of a highly electronegative dopant [48,49]. In this configuration, primary electrons liberated by the track while ionising the gas are captured at very short distances <10-100 μm by the electronegative molecules, creating negative ions. These anions drift to the anode, where their additional electron is stripped and gives rise to a standard electron avalanche. Since anions mobility depends on the mass, the difference in time of arrival of different anions effectively provides a measurement of the position of the event along the drift direction. Full 3D detector fiducialization can be obtained exploiting this information (i.e. DRIFT), and background-free operation over 1 m^3 [50]. Thanks to these two features, NITPC readout planes can image a larger volume than conventional TPC approaches, resulting in lower backgrounds and costs for unit mass.

560 SF₆ has been recently demonstrated to work very well as negative ion gas between 20 and 100 Torr, including the possibility of high gains and fiducialization via minority charge carriers [51–53]. Compared to the high vapour pressure, low flash point and low explosive mixture in air of the CS₂ employed by DRIFT, SF₆ has the substantial advantages of much more safer handling, combined with easier Radon purification and re-circulation, while at the same time increasing the target Fluorine mass. The studies proved for the first time the feasibility of NID at nearly atmospheric pressure (0.8 atm) with He/CF₄/SF₆ at 360/240/10 Torr with triple thin GEMs and charge pixel readout (Timepix) [54].

565 INITIUM goal is to develop a scintillating He/CF₄/SF₆ based gas mixture at atmospheric pressure with low content of SF₆ for NID within optical readout. If NID can be achieved within the optical approach, tracking could be improved by the possibility of reconstructing the track shape along the drift direction by sampling the recorded light at a kHz frame rate. At the moment such high rate can be met only by cameras with low resolution and high noise, not yet suited for low energy rare events searches. Nonetheless, given the fast development of the CMOS technology, advancements in **570** short time are possible which could open the door to this possibility.

5. CYGNO Scientific Goals and Expected Physics Performances

5.1. WIMP-like DM searches at low masses through nuclear recoil signature

580 A statistical analysis based on the Bayesian approach to evaluate CYGNO PHASE_1 sensitivity to WIMP searches in presence of background was performed. As input our current expectation of the detector performances, extrapolated from the experimental results obtained with prototypes discussed in Sec. 3 was employed together with the background simulations illustrated in Sec. 4.2.1.

590 In order to establish the Credible Interval (CI) of the sensitivity limits, fake experiments were simulated by extracting events according to the expected measured quantities, including detector effects. From these, the number of DM signal event posterior probability is evaluated and translated into a limit in the cross section versus mass parameters space.

595 CYGNO will measure both event energy and track directions simultaneously, and the two pieces of information will be combined into a combined fit for the final analysis. Nonetheless, since the angular distribution discriminating power is significantly stronger than the energy spectrum shape, in this sensitivity study only the first one is considered for the sake of simplicity.

600 It is important to notice how the angular distributions strongly depend on the energy threshold and the target nuclei. In this work an energy threshold of 1 keV_{ee} is assumed, backed up by the published results [34] and the improved results obtained

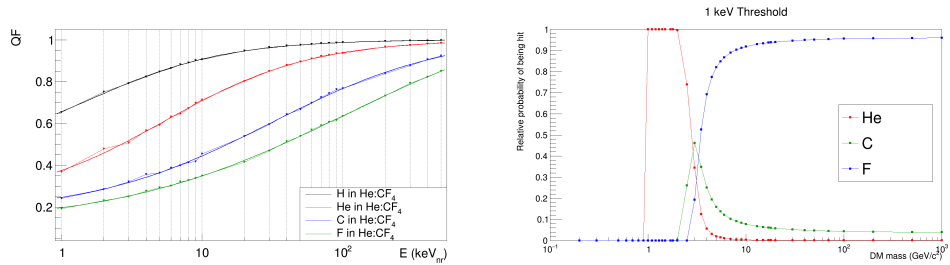


Figure 11. Left: quenching factor values for different elements in a 60/40 He/CF₄ as a function of the nuclear recoil energy E[keV_{nr}]. Right: relative probability of nuclear recoils being detected as a function of the DM mass. The energy threshold is 1 keV_{ee} and the quenching factor corrections are included.

with PHASE_0 LIME prototype (see Sec.4.1). In order to translate this into nuclear recoils energy, a SRIM simulation was developed to evaluate the quenching factor (QF) for the elements in our gas mixture. The QFs for H, He, C and F in He/CF₄ 60/40 at 1 atm as a function of the nuclear recoil energy E[keV_{nr}] is shown on the left of Fig. 11. This results in energy thresholds of 2.14 keV_{nr} for He, 3.12 keV_{nr} for C and 3.74 keV_{nr} for F.

It is interesting to notice that, due to the detector target being a mixture of different elements and to the kinematic of the expected DM-nucleus interactions, each element has a different probability of being detected depending on the DM mass. This is shown on the right of Fig. 11 and is properly taken into account in the estimation of the experiment sensitivity. The region of the DM velocity distribution accessible to detection is limited at lower values by the energy threshold and at higher by the local escape velocity. Thus, at lower DM masses, being the window of DM velocity distribution accessible very small, the detection of an element is strongly susceptible to its energy threshold. Therefore, helium detection dominates the early part of the figure and the rising probabilities of carbon and fluorine reflect their different thresholds. At higher DM masses, when the window is quite large, the A² term in the rate calculation prevails, rendering fluorine the most detectable element. Figure 11 displays also the minimum DM mass detectable by each element, that is 0.97 GeV/c² for He, 1.89 GeV/c² for C and 2.55 GeV/c² for F recoils.

While the evaluation of our approach about the directional performances on low energy nuclear recoils is still under study, from literature [55] and from the simulation within the CYGNUS effort [7] an angular resolution of 30 deg in the whole detectable range can be assumed. We furthermore recognise the capital importance of track sense recognition, as discussed, among the many, in [2,7], but for the sake of simplicity full head-tail recognition is assumed down to the 1 keV_{ee} energy threshold.

The background angular distribution will be known very well only once it is measured during data taking. It is foreseen to be partially isotropic, coming from the outside the shielding assembly, and partially structured due to presence of internal radioactive material. However, once transformed into Galactic coordinates (taking into account the rotation of the Earth and the motion of the Sun) even these structured components should dilute and the overall distribution will be isotropic at first order. The signal distributions were calculated in Galactic coordinates, starting from [56–58], neglecting the motion of the Earth as it was shown to have secondary relevance on the angular distribution. Possible shapes of the recoil distribution are shown in 2D Galactic Coordinates in Fig. 12, where it is clearly visible its an-isotropic nature. The final shape of the distribution strongly depends on three elements: the DM mass, the element hit and the energy threshold. With the chosen settings for the analysis, the angular distributions tend to be strongly peaked at low masses and more spread at heavier masses, where there is no angular region forbidden by kinematics.

As it is shown in Sec.4.2.1 the foreseen PHASE_1 detector layout and shielding will result in about 10³ NR and 5 × 10⁵ ER background events due to material radioactivity

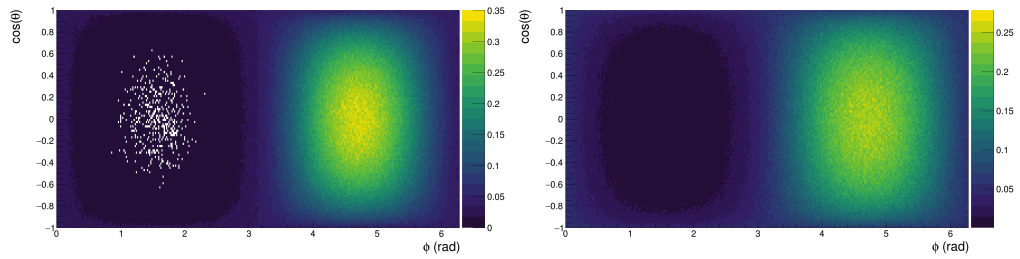


Figure 12. Two examples of the angular distribution of recoils due to DM in Galactic coordinates. On the left Helium recoils induced by $10 \text{ GeV}/\text{c}^2$ DM. On the right Fluorine recoils induced by $100 \text{ GeV}/\text{c}^2$ DM.

in the [0,20] keV range per year. All the NR are expected to be rejected through fiducialisation along the drift direction. A ER rejection factor (RF) of 10^2 has been achieved in CYGNO prototypes for electron recoils with about 6 keV energy (see Sect. 3.5) and there is room for improvements (see for example [59]). Assuming an exponential increase of the rejection factor with electron energy, an average value of O(100) background events per year can be expected in the 1-20 keV energy range, in line with what discussed above [45,46].

Given the uncertainties in these estimations and the large possibility of improvements in terms of tracking with more sophisticated approaches, the CYGNO PHASE_1 sensitivity with a background rate ranging from 10 to 10000 events per year was evaluated.

5.1.1. WIMP search Limits Evaluation and Results

For the signal prior probability, since the actual value of the cross-section of DM with protons is not known, it is difficult to produce articulated priors without risking biases. For this reason, a simple flat distribution between 0 and 1000 was used to extract the expected number of signal events. Indeed, events per year is a non negative defined variable and due to current limits in the DM community, it is hardly believable that more than 1000 events per year would be produced in the CYGNO detector.

Since the number of events surviving the signal selection is expected to be predictable with a relative good confidence (especially after the measurements foreseen in PHASE_0), for the background events a Poissonian prior centered at 10, 100, 1000 and 10000 was assumed to reflect possible different background scenarios.

For each scenario, the actual number of events is randomly extracted from this Poissonian distribution and a direction is assigned to each, randomly sampling the background angular distribution. After applying a Gaussian smearing to account for the resolution, an histogram representing the measured event direction in Galactic coordinates is filled, with its binning reflecting the angular resolution. In the hypothesis of only background, no events for the WIMP-induced signal recoils are added.

Once the data sample is prepared, the profile likelihood function is evaluated starting from the following formula:

$$p(\mathbf{D}|\mu_s, \mu_b, \boldsymbol{\theta}, H_1) = (\mu_b + \mu_s)^{N_{evt}} e^{-(\mu_b + \mu_s)} \prod_{i=1}^{N_{bins}} \left[\left(\frac{\mu_b}{\mu_b + \mu_s} P_{i,b} + \frac{\mu_s}{\mu_b + \mu_s} P_{i,s} \right)^{n_i} \frac{1}{n_i!} \right] \quad (3)$$

with:

- N_{evt} , total number of events of the data sample.
- n_i , number of events occurring in the i -th bin.
- μ , the expected events due to WIMP-induced recoil (μ_s) or background (μ_b), given a certain WIMP mass.

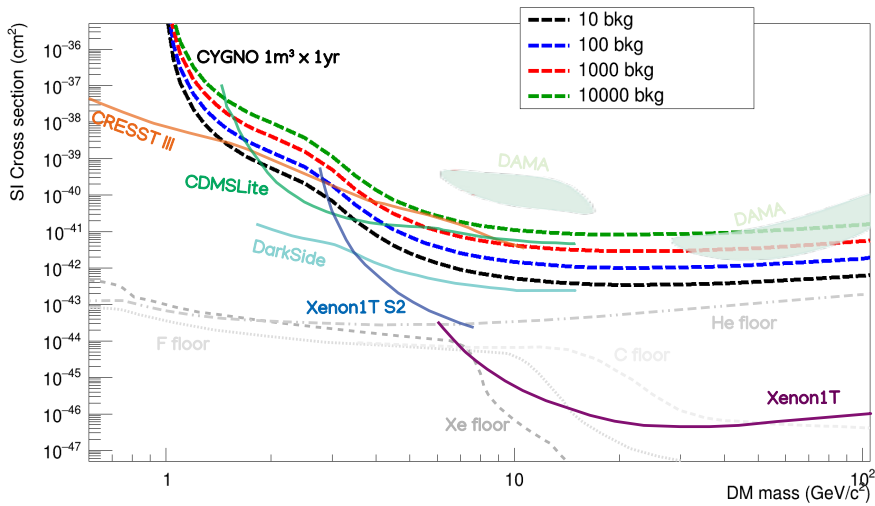


Figure 13. Spin Independent limits for WIMP-nucleon cross section for 1 m^3 CYGNO detector for 1 year exposure with different background level assumptions. The line representing other experiment are taken from [60–66].

- $P_{i,x}$, Probability of single event to end up in the i-th bin, according to x model (background or signal).

$P_{i,x}$ includes the probability due to the theoretical angular distribution, to the migration from one bin to another caused by resolution and to which element recoils. The convolution of these is summarised in templates of probabilities, generated for each of the two hypotheses.

After this step, the posterior probabilities can be computed, and $\mu_s(90\%CI)$ can be found for each DM mass and later transformed into a DM particle-proton cross section value.

To avoid the limits to suffer from any underfluctuation of the background (as undersampling), 500 data samples were created and the average result was taken as final value.

Figures 13,14 show the expected CYGNO PHASE_1 SI limits for 1 year exposure, together with some recent results by other experiments.

As it can be seen, the shape of the limit reflects the different nuclear composition of the gas mixture. The lower DM mass detectable corresponds to the one obtainable with 1 keV_{ee} energy threshold and Helium quenching factor. There is a kink on the curve at around $3\text{ GeV}/c^2$, corresponding to the transition from Helium dominated to Fluorine dominated recoils. The Carbon percentage on the total gas mixture (8%) is too low to produce a visible effect on the curve. Remarkably, both DAMA regions in the Spin Independent coupling are expected to be accessible by a 1 m^3 CYGNO detector for 1 year exposure, making this the first directional detector sensitive to that phase space region.

Thanks to the high Flourine content, CYGNO results significantly sensitive also to SD couplings, making PHASE-1 already a relevant competitor in this field, reaching performances comparable to PICO [67], as shown in Fig. 15.

As a profile likelihood function is used, the shape of the angular distribution will affect the discrimination power. The assumption that directionality is true also at the lowest energies may be a little too optimistic. When comparing CI with a regular likelihood function based on solely the number of events as in Fig. 16, it turns out that limits decrease by a factor that ranges from 1 to 4. Heavier DM masses, with more spread angular distributions are less affected, than the lighter ones. Also it can be noticed that the larger the number of background events, the stronger the effect of directionality as the lines at 10000 background event are more separated. It is important to note that,

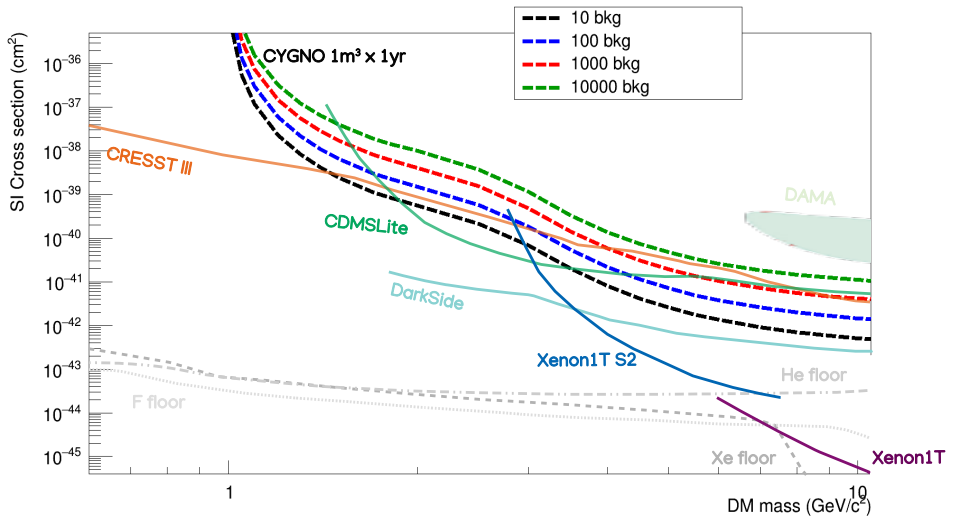


Figure 14. Spin Independent limits for WIMP-nucleon cross section for 1 m^3 CYGNO detector for 1 year exposure with different background level assumptions limited to $10 \text{ GeV}/c^2$ DM mass. The line representing other experiment are taken from [60–66].

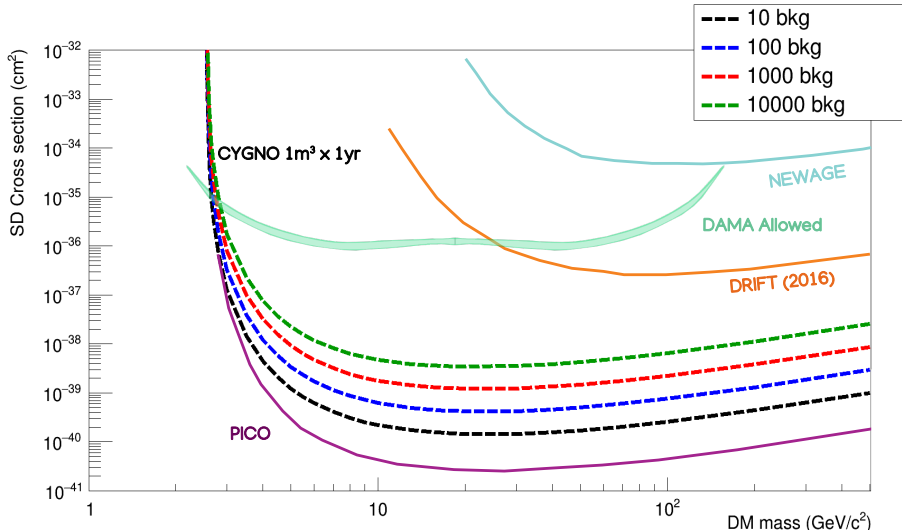


Figure 15. Spin Dependent limits for WIMP-proton cross section for 1 m^3 CYGNO detector for 1 year exposure with different background level assumptions. The line representing other experiment are taken from [67–70].

though in a loglog scale the outcome of directionality can be barely appreciated, its real strength resides in the potential for positive discovery, other than allowing the discrimination of DM models and DM astronomy after discovery [71].

5.2. Directional searches for MeV Dark Matter produced by Supernovae through nuclear recoil

While WIMPs still remains highly motivated DM candidates, they are not the only paradigm that can explain the observed DM presence. Core-collapse supernovae (SN) can reach core temperatures in excess of 30 MeV for O(10) seconds, allowing them to produce vast thermal fluxes of particles with masses O(100) MeV at relativistic speeds [72]. This makes them an ideal astrophysical source for sub-GeV dark matter. The DM candidate emerging from this scenario considered in [72] are dark fermions, but this is not the only possible realisation of such mechanism. Such particles ends up diffusively trapped near the protoneutron star that forms from the SN core. The dark fermions that

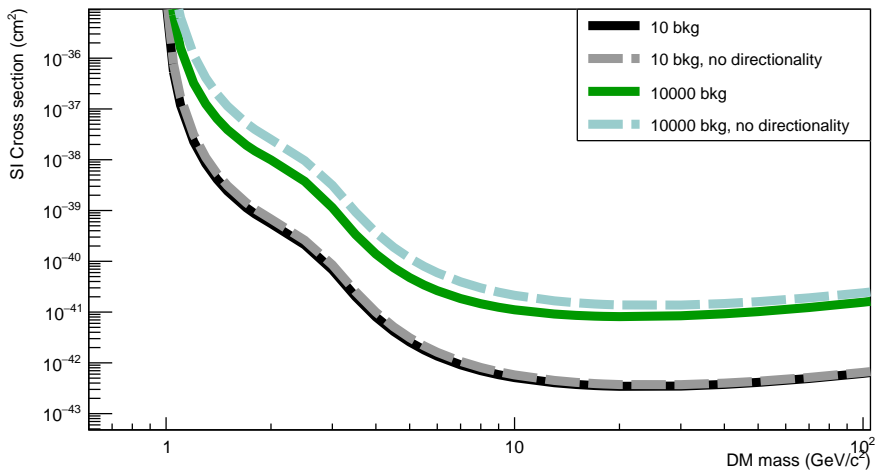


Figure 16. Comparison of the CI with and without the information of directionality. Two background configurations are considered with an exposure of $1 \text{ m}^3 \times 1 \text{ yr}$.

do eventually escape are produced with a velocity distribution approximately Maxwell-Boltzmann with semirelativistic velocities ($v \sim 1$, to be compared to classical WIMPs with $v \sim 10^{-3}$), exhibiting a roughly order-one spread in velocities. This will result in a time-spreading effect during their propagation to Earth up to 10^5 years for an average galactic SN, creating an overlap in time of various SN. Given the high SN concentration in the galactic center, the emission of > 100 SN is expected to be overlapping in a diffuse flux at Earth at any given time. This resembles the diffuse flux of SN neutrinos comprising to the Neutrino Floor at energies > 10 GeV WIMP masses.

Thanks to the large dark fermion momentum, such particles, even being of mass of O(10 MeV), would cause in a detector on Earth a measurable nuclear recoil of O(keV) very hard to distinguish from the one induced by a classic WIMP of the Galactic halo by an experiment measuring only the energy deposited in the active volume. Nonetheless, the expected diffuse flux will be strongly peaked towards the Galactic center, due to the large presence of SN in this region compared to extragalactic sources. Thanks to this high degree of anisotropy, directional detector results in a crucial tool to discriminate MeV SN-produced DM with respect to classical WIMP scenarios. It has in fact recently been shown (with participation of CYGNO collaboration members) that a directional approach with realistic experimental performances could distinguish the two scenarios with few detected signal events, typically between 1 to 2 order of magnitude with respect to the yield needed by a non-directional detector [4]. While this study was performed in the assumption of absence of background in the detect events, a full estimation of CYGNO sensitivity to this DM candidate scenario with the tools discussed developed for the WIMP physics case in Sec.5.1.1 is under development.

5.3. Solar neutrinos detection through both nuclear and electron recoil signature

Solar neutrinos are well known background to DM searches. They can interact in the active volume of the detector either via elastic scattering on the electrons (producing an electron recoil) or coherent scattering on the nuclei (producing a nuclear recoil).

Since most of current DM experiments possess ER/NR discrimination, typically only the coherent scattering on nuclei is viewed as an irreducible source background, as is in fact denominated "Neutrino Floor". Directionality has been extensively recognised as the preeminent tool to identify and discriminate NR induced by Solar neutrino from WIMP signal event [2,7,73]. While a ton-scale experiment is needed to start detecting these events [7], due to the low cross section, new physics in the neutrino sector (described in terms of new mediators between neutrinos and electrons and/or quarks or in

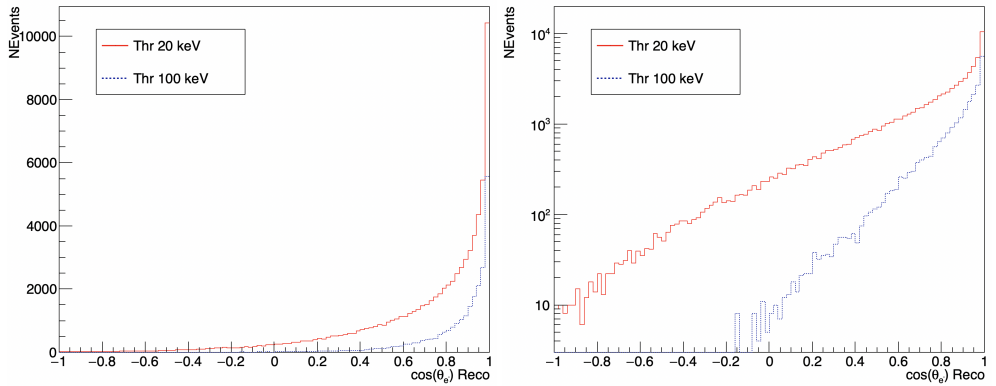


Figure 17. Angular distribution for electron recoils induced by Solar neutrinos for 20 keV and 100 keV energy threshold with a $30^\circ \times 30^\circ$ angular resolution, on the right in log scale.

755 terms of non standard effective interactions) can increase the rate at low energies [74]. This is particularly true for DM mass below 10 GeV, if a new scalar mediator is assumed, where floor can be raised by several orders of magnitude, making this accessible to CYGNO PHASE-2.

760 For what concerns ER induced by neutrino-electron elastic scattering, classical DM experiments measuring only the deposited energy in the detector have no means to discriminate them from ER caused by other sources, and hence treat them as background. Detector exhibiting directional capabilities like CYGNO can actually transform these events into a signal. From the ER direction and the Sun position, the angle between the incoming neutrino and the scattered electron can in fact be inferred, providing an 765 unambiguous signal identification just like with directional WIMP searches. Ton-scale gaseous TPC have already been proposed in the past [5,6] to perform Solar neutrino spectroscopy. The Tetrafluoromethane (CF_4) gas foreseen to be combined with He in CYGNO gas mixture due to its nice scintillation properties, appears very attractive in this sense [6], because it possess a significative electron density ($1.05 \times 10^{21} \text{ cm}^{-3}$) with 770 a low z nuclei, a feature that maximises the number of targets while minimising the multiple scattering.

775 About 1 event/ m^3 per year is expected in a He/ CF_4 60/40 gas mixture at 1 atm for an ER energy threshold of 20 keV coming from the pp chain, making this an extremely interesting physics case for CYGNO PHASE-2 experiment. Due to the larger multiple scattering suffered by low energy electron with respect to nuclei, ER direction determination results more complex than with NR tracks. First results from dedicated algorithm developed within the collaboration, inspired from X-ray polarimetry [75], shows that 30° 780 2D angular resolution with $> 80\%$ sense recognition from the sCMOS images analysis can be achieved at 20 keV in a 1 m^3 detector, improving at higher energies. Figure 17 displays the angular distribution for ER induced by Solar neutrinos for 20 keV and 100 keV energy threshold with a $30^\circ \times 30^\circ$ angular resolution. Since background events will be isotropically distributed, this shows how even with the limited angular resolution assumed, directionality provides an extremely effective means for high precision solar neutrino measurement. Moreover, the 20 keV energy threshold assumed for the ER 785 translates in about 80 keV threshold on the incoming neutrino, opening a new window of opportunity on the pp Sun process down to low energy, unreachable to conventional neutrino detectors[5].

6. Conclusions

790 In this paper, the case for directional DM searches with gaseous TPC with optical readout through the combination of sCMOS images and PMT signals is presented. The performance achieved with a 7 litres prototype based on this approach show the possibility of $O(\text{keV}_{nr})$ detection threshold with 10^2 ER/NR discrimination at 5.9 keV_{ee} . The

CYGNO experiment will develop through a staged approach, where the underground installation at LNGS of a 50 litres prototype foreseen for last quarter of 2021 will be followed by a $O(1)$ m^3 experiment. From the evaluation of the expected background rate for a $1\ m^3$ detector, properly shielded by Water and Copper, the sensitivity for PHASE_1 to WIMP searches was evaluated with different background assumptions, reflecting realistic scenarios of performances improvements or underestimation of unexpected contingencies. Additional physics cases accessible thanks to experiment directional capabilities have been discussed, for which detailed studies are under development.

The CYGNO approach results therefore highly promising and is expected to be able to significantly contribute to the advancement of TPC technology in the rare event search field.

Appendix A The Bayesian approach

The estimation of the expected limits of the CYGNO experiment was performed applying a Bayesian based method. In principle, this approach allows to calculate the probability of any model, given a certain amount of information (data) related to it. This methodology is rarely used in this field, even though it is recently gaining ground [76–83].

Every model, parameter which is of interest to the specific analysis, and experimental data are all considered connected to a probability distribution and, as such, follow the rules of probability. Exploiting the Bayes' theorem it is possible to find a relation between them and infer a final probability, called posterior, for the desired quantity. In the case of the CYGNO experiment, one is interested in knowing the number of events per year that it will be able to see. Those can be events of background (μ_b) or of signal (μ_s), which is strictly connected to the cross section of WIMP DM particle with protons. The Bayes' theorem can be expressed as follows:

$$p(\mu, \theta | D, H) = \frac{p(D|\mu, \theta, H)\pi(\mu, \theta | H)}{\int_{\Omega} \int_0^{\infty} p(D|\mu, \theta, H)\pi(\mu, \theta | H)d\mu d\theta} \quad (\text{A1})$$

with $p(D|\mu_s, \theta, H)$ representing the likelihood function $L(\mu_s, \theta)$.

In equation eq. A1, the following notation is used:

- $p(\mu|D)$, posterior probability function for the parameter μ , given D .
- $\pi(\mu)$, prior probability of a parameter. It includes the expectations of the parameters as well as constraints and knowledge previously obtained from other experiments.
- μ , free and of interest parameter representing the expected events due to WIMP-induced recoil (μ_s) or background (μ_b), given a certain WIMP mass (the analysis performs a raster scan).
- θ , vector of nuisance parameters, necessary to describe theoretical assumptions and experimental conditions that can affect the results. They can be not completely known and may depend on prior probability distributions. For example, when $\mu = \mu_s, \mu_b$, the events expected from the background, becomes a nuisance parameter.
- D , data set. Can be made of actual experimental data or simulated ones.
- H , hypothesis under test. It can be the hypothesis of pure background, H_0 , or the one where both background and signal are present, H_1 .
- Ω , nuisance parameters space.

Being in the context of estimating the limits of the CYGNO experiment when data result consistent with a pure background hypothesis, once the posterior probability of the parameter μ_s is evaluated, it is possible to compute the upper bound as the 90% Credible Interval (C.I.). This is defined as follows:

$$\mu_s(90\%CI) : \int_0^{\mu_s(90\%CI)} p(\mu_s | D, H_1) d\mu_s = 0.9 \quad (\text{A2})$$

where $p(\mu_s | D, H_1)$ is the posterior probability marginalised over the nuisance parameters. This value represents the limit under which the true value of μ_s is, with a 90% of probability.

References

1. Bertone, G.; Hooper, D.; Silk, J. Particle dark matter: Evidence, candidates and constraints. *Phys. Rept.* **2005**, *405*, 279–390, [[hep-ph/0404175](#)]. doi:10.1016/j.physrep.2004.08.031.
2. Mayet, F.; others. A review of the discovery reach of directional Dark Matter detection. *Phys. Rept.* **2016**, *627*, 1–49, [[arXiv:astro-ph.CO/1602.03781](#)]. doi:10.1016/j.physrep.2016.02.007.
3. Zurek, K.M. Asymmetric Dark Matter: Theories, Signatures, and Constraints. *Phys. Rept.* **2014**, *537*, 91–121, [[arXiv:hep-ph/1308.0338](#)]. doi:10.1016/j.physrep.2013.12.001.

4. Baracchini, E.; Derocco, W.; Dho, G. Discovering supernova-produced dark matter with directional detectors. *Phys. Rev. D* **2020**, *102*, 075036, [[arXiv:hep-ph/2009.08836](https://arxiv.org/abs/hep-ph/2009.08836)]. doi: 10.1103/PhysRevD.102.075036.
- 835 5. Seguinot, J.; Ypsilantis, T.; Zichichi, A. A High rate solar neutrino detector with energy determination. *Conf. Proc. C* **1992**, *920310*, 289–313.
6. Arpesella, C.; Broggini, C.; Cattadori, C. A possible gas for solar neutrino spectroscopy. *Astropart. Phys.* **1996**, *4*, 333–341. doi:10.1016/0927-6505(95)00051-8.
- 840 7. Vahsen, S.E.; others. CYGNUS: Feasibility of a nuclear recoil observatory with directional sensitivity to dark matter and neutrinos **2020**. [[arXiv:physics.ins-det/2008.12587](https://arxiv.org/abs/physics.ins-det/2008.12587)].
8. Marx, J.N.; Nygren, D.R. The Time Projection Chamber. *Phys. Today* **1978**, *31N10*, 46–53. doi: 10.1063/1.2994775.
9. Nygren, D.R. The Time Projection Chamber: A New 4 pi Detector for Charged Particles. *eConf* **1974**, *C740805*, 58.
- 845 10. Atwood, W.B.; others. Performance of the ALEPH time projection chamber. *Nucl. Instrum. Meth. A* **1991**, *306*, 446–458. doi:10.1016/0168-9002(91)90038-R.
11. Alme, J.; others. The ALICE TPC, a large 3-dimensional tracking device with fast readout for ultra-high multiplicity events. *Nucl. Instrum. Meth. A* **2010**, *622*, 316–367, [[arXiv:physics.ins-det/1001.1950](https://arxiv.org/abs/physics.ins-det/1001.1950)]. doi:10.1016/j.nima.2010.04.042.
- 850 12. Lippmann, C. Upgrade of the ALICE Time Projection Chamber **2014**.
13. Chardonnet, E. The DUNE dual-phase liquid argon TPC. *JINST* **2020**, *15*, C05064. doi: 10.1088/1748-0221/15/05/C05064.
14. Fraga, M.M.F.R.; Fraga, F.A.F.; Fetal, S.T.G.; Margato, L.M.S.; Ferreira-Marques, R.; Policarpo, A.J.P.L. The GEM scintillation in He CF₄, Ar CF₄, Ar TEA and Xe TEA mixtures. *Nucl. Instrum. Meth.* **2003**, *A504*, 88–92. doi:10.1016/S0168-9002(03)00758-7.
- 855 15. Margato, L.M.S.; Morozov, A.; Fraga, M.M.F.R.; Pereira, L.; Fraga, F.A.F. Effective decay time of CF₄ secondary scintillation. *JINST* **2013**, *8*, P07008. doi:10.1088/1748-0221/8/07/P07008.
16. Baracchini, E.; Benussi, L.; Bianco, S.; Capoccia, C.; Caponero, M.; Cavoto, G.; Cortez, A.; Costa, I.A.; Marco, E.D.; D'Imperio, G.; Dho, G.; Iacoangeli, F.; Maccarrone, G.; Marafini, M.; Mazzitelli, G.; Messina, A.; Orlandi, A.; Paoletti, E.; Passamonti, L.; Petrucci, F.; Piccolo, D.; Pierluigi, D.; Pinci, D.; Renga, F.; Rosatelli, F.; Russo, A.; Saviano, G.; Tomassini, S. First evidence of luminescence in a He/CF₄ gas mixture induced by non-ionizing electrons, **2020**, [[arXiv:physics.ins-det/2004.10493](https://arxiv.org/abs/physics.ins-det/2004.10493)].
- 860 17. Dominik, W.; Zaganidis, N.; Astier, P.; Charpak, G.; Santiard, J.C.; Sauli, F.; Tribollet, E.; Geissbuhler, A.; Townsend, D. A GASEOUS DETECTOR FOR HIGH ACCURACY AUTORADIOGRAPHY OF RADIOACTIVE COMPOUNDS WITH OPTICAL READOUT OF AVALANCHE POSITIONS. *Nucl. Instrum. Meth. A* **1989**, *278*, 779. doi:10.1016/0168-9002(89)91203-5.
- 865 18. Sauli, F. GEM: A new concept for electron amplification in gas detectors. *Nucl. Instrum. Meth. A* **1997**, *386*, 531–534. doi:10.1016/S0168-9002(96)01172-2.
19. Margato, L.M.S.; Fraga, F.A.F.; Fetal, S.T.G.; Fraga, M.M.F.R.; Balau, E.F.S.; Blanco, A.; Ferreira-Marques, R.; Policarpo, A.J.P.L. Performance of an optical readout GEM-based TPC. *Nucl. Instrum. Meth.* **2004**, *A535*, 231–235. doi:10.1016/j.nima.2004.07.126.
- 870 20. Marafini, M.; Patera, V.; Pinci, D.; Sarti, A.; Sciubba, A.; Spiriti, E. High granularity tracker based on a Triple-GEM optically read by a CMOS-based camera. *JINST* **2015**, *10*, P12010, [[arXiv:physics.ins-det/1508.07143](https://arxiv.org/abs/physics.ins-det/1508.07143)]. doi:10.1088/1748-0221/10/12/P12010.
21. Phan, N.S.; Lee, E.R.; Loomba, D. Imaging ⁵⁵Fe Electron Tracks in a GEM-based TPC Using a CCD Readout. *arXiv* **1703.09883** **2017**, [[arXiv:physics.ins-det/1703.09883](https://arxiv.org/abs/physics.ins-det/1703.09883)].
- 875 22. Fraga, F.A.F.; Margato, L.M.S.; Fetal, S.T.; Fraga, M.M.F.R.; Ferreira-Marques, R.; Policarpo, A.J.P.L.; Guerard, B.; Oed, A.; Manzini, G.; van Vuure, T. CCD readout of GEM-based neutron detectors. *Nucl. Instrum. Meth. A* **2002**, *478*, 357–361. doi:10.1016/S0168-9002(01)01829-0.
23. Mavrokoridis, K.; Ball, F.; Carroll, J.; Lazos, M.; McCormick, K.J.; Smith, N.A.; Touramanis, C.; Walker, J. Optical Readout of a Two Phase Liquid Argon TPC using CCD Camera and THGEMs. *JINST* **2014**, *9*, P02006, [[arXiv:physics.ins-det/1401.0525](https://arxiv.org/abs/physics.ins-det/1401.0525)]. doi:10.1088/1748-0221/9/02/P02006.
- 880 24. Marafini, M.; Patera, V.; Pinci, D.; Sarti, A.; Sciubba, A.; Spiriti, E. ORANGE: A high sensitivity particle tracker based on optically read out GEM. *Nucl. Instrum. Meth.* **2017**, *A845*, 285–288. doi:10.1016/j.nima.2016.04.014.

- 890 25. Antochi, V.C.; Baracchini, E.; Cavoto, G.; Marco, E.D.; Marafini, M.; Mazzitelli, G.; Pinci, D.; Renga, F.; Tomassini, S.; Voena, C. Combined readout of a triple-GEM detector. *JINST* **2018**, *13*, P05001, [[arXiv:physics.ins-det/1803.06860](https://arxiv.org/abs/physics/ins-det/1803.06860)]. doi:10.1088/1748-0221/13/05/P05001.
- 895 26. Marafini, M.; Patera, V.; Pinci, D.; Sarti, A.; Sciubba, A.; Torchia, N.M. Study of the Performance of an Optically Readout Triple-GEM. *IEEE Transactions on Nuclear Science* **2018**, *65*, 604–608. doi:10.1109/TNS.2017.2778503.
- 900 27. Pinci, D.; Baracchini, E.; Cavoto, G.; Marco, E.D.; Marafini, M.; Mazzitelli, G.; Renga, F.; Tomassini, S.; Voena, C. High resolution TPC based on optically readout GEM. *Nuclear Instruments and Methods in Physics Research Section A: Accelerators, Spectrometers, Detectors and Associated Equipment* **2018**. doi:<https://doi.org/10.1016/j.nima.2018.11.085>.
- 905 28. Antochi, V.C.; Cavoto, G.; Costa, I.A.; Marco, E.D.; D'Imperio, G.; Iacoangeli, F.; Marafini, M.; Messina, A.; Pinci, D.; Renga, F.; Voena, C.; Baracchini, E.; Cortez, A.; Dho, G.; Benussi, L.; Bianco, S.; Capoccia, C.; Caponero, M.; Maccarrone, G.; Mazzitelli, G.; Orlandi, A.; Paoletti, E.; Passamonti, L.; Piccolo, D.; Pierluigi, D.; Rosatelli, F.; Russo, A.; Saviano, G.; Tomassini, S.; Nobrega, R.A.; Petrucci, F. A GEM-based Optically Readout Time Projection Chamber for charged particle tracking, 2020, [[arXiv:physics.ins-det/2005.12272](https://arxiv.org/abs/physics/ins-det/2005.12272)].
- 910 29. Costa, I.A.; Baracchini, E.; Bellini, F.; Benussi, L.; Bianco, S.; Caponero, M.; Cavoto, G.; D'Imperio, G.; Marco, E.D.; Maccarrone, G.; Marafini, M.; Mazzitelli, G.; Messina, A.; Petrucci, F.; Piccolo, D.; Pinci, D.; Renga, F.; Rosatelli, F.; Saviano, G.; Tomassini, S. Stability and detection performance of a GEM-based Optical Readout TPC with He/CF₄ gas mixtures. *Journal of Instrumentation* **2020**, *xx*, xxx. doi:yyy.
- 915 30. Campagnola, R. Study and optimization of the light-yield of a triple-GEM detector **2018**.
31. Veenhof, R. Garfield, a drift chamber simulation program. *Conf. Proc. C* **1993**, *9306149*, 66–71.
- 920 32. Veenhof, R. GARFIELD, recent developments. *Nucl. Instrum. Meth. A* **1998**, *419*, 726–730. doi:10.1016/S0168-9002(98)00851-1.
- 925 33. Agostinelli, S.; others. GEANT4: A Simulation toolkit. *Nucl. Instrum. Meth. A* **2003**, *506*, 250–303. doi:10.1016/S0168-9002(03)01368-8.
34. Costa, I.A.; Baracchini, E.; Bellini, F.; Benussi, L.; Bianco, S.; Caponero, M.; Cavoto, G.; D'Imperio, G.; Marco, E.D.; Maccarrone, G.; Marafini, M.; Mazzitelli, G.; Messina, A.; Petrucci, F.; Piccolo, D.; Pinci, D.; Renga, F.; Rosatelli, F.; Saviano, G.; Tomassini, S. Performance of optically readout GEM-based TPC with a 55Fe source. *Journal of Instrumentation* **2019**, *14*, P07011–P07011. doi:10.1088/1748-0221/14/07/p07011.
- 930 35. Antochi, V.; Baracchini, E.; Benussi, L.; Bianco, S.; Capoccia, C.; Caponero, M.; Cavoto, G.; Cortez, A.; Costa, I.; Di Marco, E.; et al.. Performance of an optically read out time projection chamber with ultra-relativistic electrons. *Nuclear Instruments and Methods in Physics Research Section A: Accelerators, Spectrometers, Detectors and Associated Equipment* **2021**, *999*, 165209, [[arXiv:physics.ins-det/2005.12272v3](https://arxiv.org/abs/physics/ins-det/2005.12272v3)]. doi:10.1016/j.nima.2021.165209.
- 935 36. B.Buonomo.; C.Di Giulio.; L.G.Foggetta.; P.Valente. A Hardware and Software Overview on the New BTF Transverse Profile Monitor. Proc. 5th Int. Beam Instrumentation Conf. (IBIC'16), Barcelona, Spain, 2016, pp. 818–821. doi:10.18429/JACoW-IBIC2016-WEPG73.
- 940 37. P.Valente.; B.Buonomo.; Di Giulio, C.; L.G.Foggetta. Frascati Beam-Test Facility (BTF) High Resolution Beam Spot Diagnostics. Proc. 5th Int. Beam Instrumentation Conf. (IBIC'16), Barcelona, Spain, 2016, pp. 222–225. doi:10.18429/JACoW-IBIC2016-MOPG65.
38. Blum, W.; Rolandi, L.; Riegler, W. *Particle detection with drift chambers; Particle Acceleration and Detection*, ISBN = 9783540766834, 2008. doi:10.1007/978-3-540-76684-1.
- 945 39. Baracchini, E.; others. A density-based clustering algorithm for the CYGNO data analysis. *JINST* **2020**, *15*, T12003, [[arXiv:physics.ins-det/2007.01763](https://arxiv.org/abs/physics/ins-det/2007.01763)]. doi:10.1088/1748-0221/15/12/T12003.
40. Ester, M.; Kriegel, H.P.; Sander, J.; Xu, X. A Density-based Algorithm for Discovering Clusters a Density-based Algorithm for Discovering Clusters in Large Spatial Databases with Noise. Proceedings of the Second International Conference on Knowledge Discovery and Data Mining. AAAI Press, 1996, KDD'96, pp. 226–231.
41. Baracchini, E.; others. Identification of low energy nuclear recoils in a gas TPC with optical readout **2020**. [[arXiv:physics.ins-det/2007.12508](https://arxiv.org/abs/physics/ins-det/2007.12508)]. doi:10.1088/1361-6501/abbd12.
42. Battat, J.B.R.; others. Reducing DRIFT Backgrounds with a Submicron Aluminized-Mylar Cathode. *Nucl. Instrum. Meth. A* **2015**, *794*, 33–46, [[arXiv:physics.ins-det/1502.03535](https://arxiv.org/abs/physics/ins-det/1502.03535)]. doi:10.1016/j.nima.2015.04.070.
43. Akl, M.A.; others. CMS Technical Design Report for the Muon Endcap GEM Upgrade **2015**.

44. Benussi, L.; Bianco, S.; Caponero, M.; Muhammad, S.; Passamonti, L.; Piccolo, D.; Pierluigi, D.; Raffone, G.; Russo, A.; Saviano, G. Fiber Bragg Grating sensors for deformation monitoring of GEM foils in HEP detectors. 6th IEEE International Workshop on Advances in Sensors and Interfaces, 2015, [[arXiv:physics.ins-det/1512.08629](#)]. doi:10.1109/IWASL.2015.7184954.
45. Riffard, Q.; others. MIMAC low energy electron-recoil discrimination measured with fast neutrons. *JINST* **2016**, *11*, P08011, [[arXiv:astro-ph.IM/1602.01738](#)]. doi:10.1088/1748-0221/11/08/P08011.
46. Phan, N.S.; Lauer, R.J.; Lee, E.R.; Loomba, D.; Matthews, J.A.J.; Miller, E.H. GEM-based TPC with CCD Imaging for Directional Dark Matter Detection. *Astropart. Phys.* **2016**, *84*, 82–96, [[arXiv:physics.ins-det/1510.02170](#)]. doi:10.1016/j.astropartphys.2016.08.006.
47. Baracchini, E.; others. First evidence of luminescence in a He/CF₄ gas mixture induced by non-ionizing electrons. *JINST* **2020**, *15*, P08018, [[arXiv:physics.ins-det/2004.10493](#)]. doi:10.1088/1748-0221/15/08/P08018.
48. Martoff, C.J.; Snowden-Ifft, D.P.; Ohnuki, T.; Spooner, N.; Lehner, M. Suppressing drift chamber diffusion without magnetic field. *Nucl. Instrum. Meth. A* **2000**, *440*, 355–359. doi:10.1016/S0168-9002(99)00955-9.
49. Ohnuki, T.; Snowden-Ifft, D.P.; Martoff, C.J. Measurement of carbon disulfide anion diffusion in a TPC. *Nucl. Instrum. Meth. A* **2001**, *463*, 142–148, [[physics/0004006](#)]. doi:10.1016/S0168-9002(01)00222-4.
50. Battat, J.B.R.; others. Low Threshold Results and Limits from the DRIFT Directional Dark Matter Detector. *Astropart. Phys.* **2017**, *91*, 65–74, [[arXiv:astro-ph.IM/1701.00171](#)]. doi:10.1016/j.astropartphys.2017.03.007.
51. Phan, N.S.; Lafler, R.; Lauer, R.J.; Lee, E.R.; Loomba, D.; Matthews, J.A.J.; Miller, E.H. The novel properties of SF₆ for directional dark matter experiments. *JINST* **2017**, *12*, P02012, [[arXiv:physics.ins-det/1609.05249](#)]. doi:10.1088/1748-0221/12/02/P02012.
52. Ikeda, T.; Shimada, T.; Ishiura, H.; Nakamura, K.D.; Nakamura, T.; Miuchi, K. Development of a negative ion micro TPC detector with SF₆ gas for the directional dark matter search. *JINST* **2020**, *15*, P07015, [[arXiv:physics.ins-det/2004.09706](#)]. doi:10.1088/1748-0221/15/07/P07015.
53. Lightfoot, P.K.; Spooner, N.J.C.; Lawson, T.B.; Aune, S.; Giomataris, I. First operation of bulk micromegas in low pressure negative ion drift gas mixtures for dark matter searches. *Astropart. Phys.* **2007**, *27*, 490–499. doi:10.1016/j.astropartphys.2007.02.003.
54. Baracchini, E.; Cavoto, G.; Mazzitelli, G.; Murtas, F.; Renga, F.; Tomassini, S. Negative Ion Time Projection Chamber operation with SF₆ at nearly atmospheric pressure. *JINST* **2018**, *13*, P04022, [[arXiv:physics.ins-det/1710.01994](#)]. doi:10.1088/1748-0221/13/04/P04022.
55. Nakamura, K.; others. Low pressure gas study for a direction-sensitive dark matter search experiment with MPGD. *JINST* **2012**, *7*, C02023. doi:10.1088/1748-0221/7/02/C02023.
56. Lewin, J.; Smith, P. Review of mathematics, numerical factors, and corrections for dark matter experiments based on elastic nuclear recoil. *Astroparticle Physics* **1996**, *6*, 87–112. doi:[https://doi.org/10.1016/S0927-6505\(96\)00047-3](https://doi.org/10.1016/S0927-6505(96)00047-3).
57. Gondolo, P. Recoil momentum spectrum in directional dark matter detectors. *Physical Review D* **2002**, *66*, [[arXiv:hep-ph/0209110v2](#)]. doi:10.1103/physrevd.66.103513.
58. Baxter, D.; Bloch, I.M.; Bodnia, E.; Chen, X.; Conrad, J.; Gangi, P.D.; Dobson, J.E.Y.; Durnford, D.; Haselschwardt, S.J.; Kaboth, A.; Lang, R.F.; Lin, Q.; Lippincott, W.H.; Liu, J.; Manalaysay, A.; McCabe, C.; Mora, K.D.; Naim, D.; Neilson, R.; Olcina, I.; Piro, M.C.; Selvi, M.; von Krosigk, B.; Westerdale, S.; Yang, Y.; Zhou, N. Recommended conventions for reporting results from direct dark matter searches, 2021, [[arXiv:hep-ex/2105.00599v1](#)].
59. Vahsen, S.E.; O'Hare, C.A.J.; Lynch, W.A.; Spooner, N.J.C.; Baracchini, E. CYGNUS: Feasibility of a nuclear recoil observatory with directional sensitivity to dark matter and neutrinos. *arXiv:2008.12587*.
60. Aprile, E.; Aalbers, J.; Agostini, F.; Alfonsi, M.; Althueser, L.; Amaro, F.; Anthony, M.; Arneodo, F.; Baudis, L.; Bauermeister, B.; et al.. Dark Matter Search Results from a One Ton-Year Exposure of XENON1T. *Physical Review Letters* **2018**, *121*, [[arXiv:astro-ph.CO/1805.12562v2](#)]. doi:10.1103/physrevlett.121.111302.
61. Aprile, E.; Aalbers, J.; Agostini, F.; Alfonsi, M.; Althueser, L.; Amaro, F.; Antochi, V.; Angelino, E.; Arneodo, F.; Barge, D.; et al.. Light Dark Matter Search with Ionization Signals in XENON1T. *Physical Review Letters* **2019**, *123*, [[arXiv:hep-ex/1907.11485v2](#)]. doi:10.1103/physrevlett.123.251801.

62. Boehm, C.; Cerdeño, D.; Machado, P.; Campo, A.O.D.; Reid, E. How high is the neutrino floor? *Journal of Cosmology and Astroparticle Physics* **2019**, *2019*, 043–043, [[arXiv:hep-ph/1809.06385v4](#)]. doi:10.1088/1475-7516/2019/01/043.
- 1010 63. Agnes, P.; Albuquerque, I.; Alexander, T.; Alton, A.; Araujo, G.; Asner, D.; Ave, M.; Back, H.; Baldin, B.; Batignani, G.; et al.. Low-Mass Dark Matter Search with the DarkSide-50 Experiment. *Physical Review Letters* **2018**, *121*, [[arXiv:astro-ph.HE/1802.06994v3](#)]. doi:10.1103/physrevlett.121.081307.
- 1015 64. Agnese, R.; Anderson, A.; Aralis, T.; Aramaki, T.; Arnquist, I.; Baker, W.; Balakishiyeva, D.; Barker, D.; Basu Thakur, R.; Bauer, D.; et al.. Low-mass dark matter search with CDMSlite. *Physical Review D* **2018**, *97*, [[arXiv:astro-ph.CO/1707.01632v3](#)]. doi:10.1103/physrevd.97.022002.
65. Mancuso, M.; others. Searches for Light Dark Matter with the CRESST-III Experiment. *J. Low Temp. Phys.* **2020**, *199*, 547–555. doi:10.1007/s10909-020-02343-3.
- 1020 66. Savage, C.; Gelmini, G.; Gondolo, P.; Freese, K. Compatibility of DAMA/LIBRA dark matter detection with other searches. *Journal of Cosmology and Astroparticle Physics* **2009**, *2009*, 010–010, [[arXiv:astro-ph/0808.3607v3](#)]. doi:10.1088/1475-7516/2009/04/010.
- 1025 67. Amole, C.; Ardid, M.; Arnquist, I.; Asner, D.; Baxter, D.; Behnke, E.; Bressler, M.; Broerman, B.; Cao, G.; Chen, C.; et al.. Dark matter search results from the complete exposure of the PICO-60 C3F8 bubble chamber. *Physical Review D* **2019**, *100*, [[arXiv:astro-ph.CO/1902.04031v1](#)]. doi:10.1103/physrevd.100.022001.
68. Savage, C.; Gondolo, P.; Freese, K. Can WIMP spin dependent couplings explain DAMA data, in light of null results from other experiments? *Physical Review D* **2004**, *70*, [[arXiv:astro-ph/0408346v3](#)]. doi:10.1103/physrevd.70.123513.
- 1030 69. Battat, J.; Ezereibe, A.; Gauvreau, J.L.; Harton, J.; Lafler, R.; Law, E.; Lee, E.; Loomba, D.; Lumnah, A.; Miller, E.; et al.. Low threshold results and limits from the DRIFT directional dark matter detector. *Astroparticle Physics* **2017**, *91*, 65–74, [[arXiv:astro-ph.IM/1701.00171v3](#)]. doi:10.1016/j.astropartphys.2017.03.007.
- 1035 70. Yakabe, R.; Nakamura, K.; Ikeda, T.; Ito, H.; Yamaguchi, Y.; Taishaku, R.; Nakazawa, M.; Ishiura, H.; Nakamura, T.; Shimada, T.; Tanimori, T.; Kubo, H.; Takada, A.; Sekiya, H.; Takeda, A.; Miuchi, K. First limits from a 3d-vector directional dark matter search with the NEWAGE-0.3b' detector, 2020, [[arXiv:hep-ex/2005.05157](#)].
- 1040 71. Baracchini, E.; DeRocco, W.; Dho, G. Discovering supernova-produced dark matter with directional detectors. *Physical Review D* **2020**, *102*, [[arXiv:hep-ph/2009.08836v1](#)]. doi:10.1103/physrevd.102.075036.
72. DeRocco, W.; Graham, P.W.; Kasen, D.; Marques-Tavares, G.; Rajendran, S. Supernova signals of light dark matter. *Phys. Rev. D* **2019**, *100*, 075018, [[arXiv:hep-ph/1905.09284](#)]. doi:10.1103/PhysRevD.100.075018.
- 1045 73. Billard, J.; Strigari, L.; Figueroa-Feliciano, E. Implication of neutrino backgrounds on the reach of next generation dark matter direct detection experiments. *Phys. Rev. D* **2014**, *89*, 023524, [[arXiv:hep-ph/1307.5458](#)]. doi:10.1103/PhysRevD.89.023524.
74. Boehm, C.; Cerdeño, D.G.; Machado, P.A.N.; Olivares-Del Campo, A.; Perdomo, E.; Reid, E. How high is the neutrino floor? *JCAP* **2019**, *01*, 043, [[arXiv:hep-ph/1809.06385](#)]. doi:10.1088/1475-7516/2019/01/043.
- 1050 75. Soffitta, P.; Muleri, F.; Fabiani, S.; Costa, E.; Bellazzini, R.; Brez, A.; Minuti, M.; Pinchera, M.; Spandre, G. Measurement of the position resolution of the Gas Pixel Detector. *Nucl. Instrum. Meth. A* **2013**, *700*, 99–105, [[arXiv:astro-ph.IM/1208.6330](#)]. doi:10.1016/j.nima.2012.09.055.
76. Roszkowski, L.; Ruiz de Austri, R.; Silk, J.; Trotta, R. On prospects for dark matter indirect detection in the Constrained MSSM. *Physics Letters B* **2009**, *671*, 10–14, [[0707.0622v2](#)]. doi:https://doi.org/10.1016/j.physletb.2008.11.061.
- 1055 77. Trotta, R.; de Austri, R.R.; Roszkowski, L. Prospects for direct dark matter detection in the constrained MSSM. *New Astronomy Reviews* **2007**, *51*, 316–320, [[arXiv:astro-ph/0609126v1](#)]. Francesco Melchiorri: Scientist, Pioneer, Mentor, doi:https://doi.org/10.1016/j.newar.2006.11.059.
78. Stuge, C.; Trotta, R.; Bertone, G.; Peter, A.H.G.; Scott, P. Fundamental statistical limitations of future dark matter direct detection experiments. *Physical Review D* **2012**, *86*, [[arXiv:hep-ph/1201.3631v2](#)]. doi:10.1103/physrevd.86.023507.
- 1060 79. Arina, C. Bayesian analysis of multiple direct detection experiments, 2014, [[arXiv:hep-ph/1310.5718](#)].
80. Bringmann, T.; Conrad, J.; Cornell, J.M.; Dal, L.A.; Edsjö, J.; Farmer, B.; Kahlhoefer, F.; Kvellestad, A.; Putze, A.; et al.. DarkBit: a GAMBIT module for computing dark mat-

- ¹⁰⁶⁵ ter observables and likelihoods. *The European Physical Journal C* **2017**, *77*, [[arXiv:hep-ph/1705.07920v2](#)]. doi:10.1140/epjc/s10052-017-5155-4.
81. Liem, S.; Bertone, G.; Calore, F.; de Austri, R.R.; Tait, T.M.P.; Trotta, R.; Weniger, C. Effective field theory of dark matter: a global analysis. *Journal of High Energy Physics* **2016**, *2016*, [[arXiv:hep-ph/1603.05994v1](#)]. doi:10.1007/jhep09(2016)077.
- ¹⁰⁷⁰ 82. Messina, A.; Nardecchia, M.; Piacentini, S. Annual modulations from secular variations: not relaxing DAMA? *Journal of Cosmology and Astroparticle Physics* **2020**, *2020*, 037–037, [[arXiv:hep-ph/2003.03340v2](#)]. doi:10.1088/1475-7516/2020/04/037.
- ¹⁰⁷⁵ 83. di Cortona, G.G.; Messina, A.; Piacentini, S. Migdal effect and photon Bremsstrahlung: improving the sensitivity to light dark matter of liquid argon experiments. *Journal of High Energy Physics* **2020**, *2020*, [[arXiv:hep-ph/2006.02453v2](#)]. doi:10.1007/jhep11(2020)034.

